The Astrophysical Journal, 752:59 (18pp), 2012 June 10 doi:10.1088/0004-637X/752/1/59

THE LOW-MASS STELLAR POPULATION IN L1641: EVIDENCE FOR ENVIRONMENTAL DEPENDENCE OF THE STELLAR INITIAL MASS FUNCTION

Wen-Hsin Hsu[1], Lee Hartmann[1], Lori Allen[2], Jesús Hernández[3], S. T. Megeath[4], Gregory Mosby[5], John J. Tobin[6], and Catherine Espaillat[7]
[1] Department of Astronomy, University of Michigan, 500 Church St., Ann Arbor, MI 48109, USA
[2] National Optical Astronomy Observatory, 950 North Cherry Ave., Tucson, AZ 85719, USA
[3] Centro de Investigaciones de Astronomía, Apdo. Postal 264, Mérida 5101-A, Venezuela
[4] Department of Physics and Astronomy, University of Toledo, 2801 West Bancroft Street, Toledo, OH 43606, USA
[5] Department of Astronomy, University of Wisconsin-Madison, 475 N. Charter Street, Madison, WI 53706, USA
[6] National Radio Astronomy Observatory, 520 Edgemont Road, Charlottesville, VA 22903, USA
[7] Harvard-Smithsonian Center for Astrophysics, 60 Garden Street, MS-78, Cambridge, MA 02138, USA
Received 2012 February 1; accepted 2012 April 12; published 2012 May 25

ABSTRACT

We present results from an optical photometric and spectroscopic survey of the young stellar population in L1641, the low-density star-forming region of the Orion A cloud south of the Orion Nebula Cluster (ONC). Our goal is to determine whether L1641 has a large enough low-mass population to make the known lack of high-mass stars a statistically significant demonstration of environmental dependence of the upper mass stellar initial mass function (IMF). Our spectroscopic sample consists of IR-excess objects selected from the *Spitzer*/IRAC survey and non-excess objects selected from optical photometry. We have spectral confirmation of 864 members, with another 98 probable members; of the confirmed members, 406 have infrared excesses and 458 do not. Assuming the same ratio of stars with and without IR excesses in the highly extincted regions, L1641 may contain as many as ∼1600 stars down to ∼0.1 $M_{\odot}$, comparable within a factor of two to the ONC. Compared to the standard models of the IMF, L1641 is deficient in O and early B stars to a 3σ–4σ significance level, assuming that we know of all the massive stars in L1641. With a forthcoming survey of the intermediate-mass stars, we will be in a better position to make a direct comparison with the neighboring, dense ONC, which should yield a stronger test of the dependence of the high-mass end of the stellar IMF on environment.

Key words: stars: formation – stars: low-mass – stars: luminosity function, mass function – stars: pre-main sequence – surveys

Online-only material: color figures, machine-readable tables

1. INTRODUCTION

Do the most massive stars form preferentially in dense, massive environments? Answering this question has proved to be frustratingly difficult. The recent review by Bastian et al. (2010) concludes that there is no clear evidence for nonstandard stellar initial mass functions (IMFs) in specific environments, though this issue "clearly warrant(s) further study." One problem is that most of the studies of IMFs in relatively unevolved young regions have been conducted on young star clusters (Bastian et al. 2010; Weidner et al. 2010, and references therein), because it is much more difficult to study low-density, dispersed regions. Perhaps the most extensive survey to date on star formation in low-density environments is that of Luhman et al. (2009), which argued that samples of roughly 150 and 300 members of Taurus (depending on the region surveyed) showed an anomalous IMF, particularly in suggesting a peak near spectral types K7–M0 not observed in other regions. However, the low-mass population of Taurus is insufficiently numerous to make a strong test of the high-mass end of the IMF.

The lower part of the Orion A molecular cloud, south of the Orion Nebula Cluster (ONC) region, appears to be one site where a significant test of the dependence of the upper mass distribution in a lower-density environment can be carried out. For simplicity we call this region "L1641," though this is a broader use of the original Lynds cloud designation (as discussed further in Section 4.2; also see Allen & Davis 2008 for a discussion of the individual clouds). As the lower part of the Orion A cloud is contiguous with the ONC region, it can be assumed that L1641 is at roughly the same distance as the ONC (∼420 pc; Menten et al. 2007; Kim et al. 2008), allowing the stellar populations of the two regions to be compared directly. Based on previous surveys, as well as the recent *Spitzer*/IRAC survey of infrared-excess stars (see Figure 1 for locations of the IR-excess objects; data to be published in S. T. Megeath et al. 2012, in preparation), it appears that L1641 contains a much larger pre-main-sequence population than other nearby low-density regions such as Taurus–Auriga (see, e.g., Luhman et al. 2009; Rebull et al. 2011).

The star of earliest spectral type spatially associated with the molecular gas south of $-6\overset{\circ}{.}1$ declination is B4 (Racine 1968), with only an additional 12 late B stars projected on the cloud according to current surveys (Skiff 2010). The ONC, on the other hand, has two O stars and seven stars with spectral types earlier than B4, and its IMF is consistent with a Salpeter upper mass slope (Muench et al. 2002; Da Rio et al. 2009). The question to be addressed is whether this apparent deficit of high-mass stars in L1641 is the result of its being a relatively low-density environment, in contrast to the densely clustered ONC, or whether L1641 simply does not have enough members in comparison with the ONC (with ∼2000 members; Hillenbrand & Hartmann 1998; Muench et al. 2002; Da Rio et al. 2009; Robberto et al. 2010) that high-mass stars are probable, assuming a universal IMF.

In this paper, we present optical *V*- and *I*-band photometry and low-resolution optical spectroscopy of low-mass stars in L1641. We estimate that there are about 1600 low-mass members in the region, assuming that the disk fraction is constant throughout

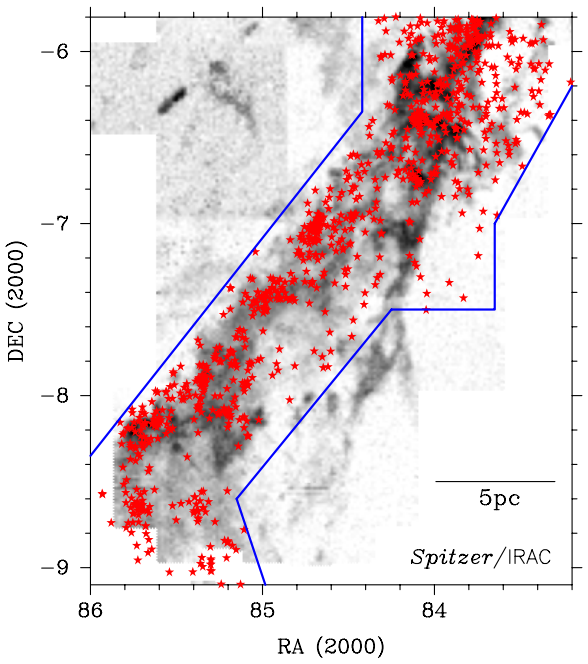

Figure 1. Blue boundary lines represent the fields covered by the *Spitzer*/IRAC survey of Orion (S. T. Megeath et al. 2012, in preparation), and the red stars show IR-excess objects identified by this survey, which are overlaid on the ^{13}CO map from Bally et al. (1987). The physical scale of 5 pc is also shown in the plot, assuming a distance of 420 pc.

(A color version of this figure is available in the online journal.)

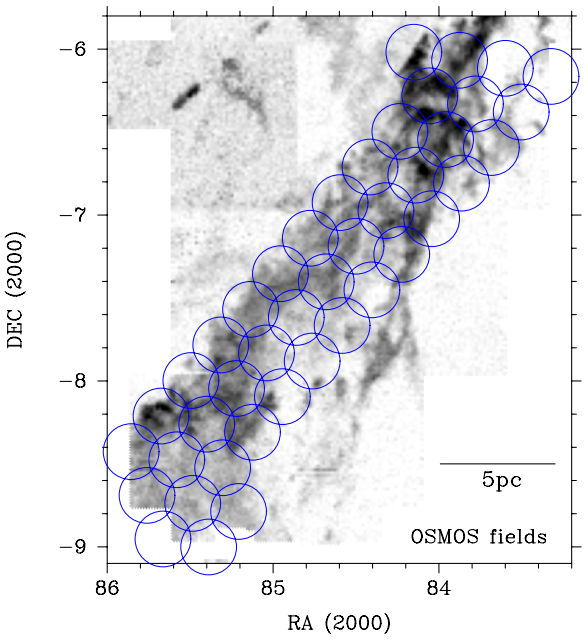

Figure 2. OSMOS optical photometry fields (blue circles) overlaid on the ^{13}CO map (Bally et al. 1987). The physical scale of 5 pc is also shown in the plot, assuming a distance of 420 pc.

(A color version of this figure is available in the online journal.)

the cloud. Furthermore, we show that the average age of the stars in our sample is only slightly greater than that of the ONC region. Thus, our findings support the idea that the comparison between L1641 and the ONC ultimately will provide a good test of the possible environmental dependence of the upper mass IMF. For this paper, we consider O and B stars found in the literature and assume that there are no deeply embedded early B stars that we do not already know. Under this assumption, we then make comparisons with standard forms of the IMF, which indicate that L1641 is deficient in early B and O stars, based on the known low-mass population. In a forthcoming paper, we will discuss our search for high-mass members and add intermediate-mass members verified by spectroscopy, which are currently missing from our sample. In Section 2, we describe our observational program and the procedures used to reduce the data. In Section 3, we present an analysis of our photometric and spectroscopic results. Then in Section 4, we summarize our knowledge of the low-mass population, briefly relate our results to the known population of early-type stars, consider some uncertainties related to deciding where to divide the region between low- and high-density areas, and make some preliminary tests using standard models of the IMF. Finally, we present our conclusions in Section 5.

2. OBSERVATIONS AND DATA REDUCTION

2.1. Optical Photometry

We obtained *V*- and *I*-band optical photometry with the Ohio State Multi-Object Spectrograph (OSMOS) on the MDM 2.4 m Hiltner telescope (Stoll et al. 2010; Martini et al. 2011). The detector has a 18.′5 × 18.′5 field of view, vignetted by a 20′ diameter circle. We used 2 × 2 binning, which gives a plate scale of 0.″55 pixel^{-1}. The majority of L1641 from −6° to −9.°2 was covered with 41 fields (see Figure 2). The exposure sequence consists of one short exposure (5 seconds) and two long exposures (60 seconds) in both *V* and *I* bands. The photometry was obtained on the nights of 2010 December 7–8 and December 8–9. Most fields were observed with the exposure sequence once on each night, but a few fields were only observed on one night. The conditions were not completely photometric, with some visible cirrus at the beginning of each night, and the seeing ranged from 1.″1 to 1.″8 FWHM. However, we started observing L1641 3–4 hr after twilight ended, and most of the cirrus had disappeared by then. We observed two Landolt standard fields every 2 hr throughout the night for photometric calibration. SA92, SA95, SA98, and SA101 were used according to the time of the night.

Each CCD frame was first corrected by overscan using the IDL program proc4k written by Jason Eastman. Note that the original program is written for the Ohio State 4k CCD imager alone and has been modified to process OSMOS data. We then performed the basic reduction following the standard procedure using IRAF. Note that we used sky flats in the flat-field correction. We determined the astrometric solution with *imwcs* in *WCSTools*, using the coordinates of stars from the Two Micron All Sky Survey (2MASS) catalog. The astrometric solutions are in general good within one pixel, or 0.″55. We then obtained aperture photometry with the IRAF *phot* package, using an aperture of 8, or ∼3–4 times the FWHM. We used the Landolt fields for photometric calibrations. The rms departures of the standard stars from the calibration equations are ∼0.05 mag for both *V* and *I* bands. The MDM 4k imager used by OSMOS has a known issue of crosstalk between the four CCD segments. When a CCD pixel is saturated, it creates spurious point sources in corresponding pixels on the other three segments. Therefore, instead of finding point sources in the images with *daofind*-like packages, we used the positions of all 2MASS point sources for our photometry. Non-detections and saturated stars in either bands are removed. If a star is saturated in the long exposure but not in the short exposure,

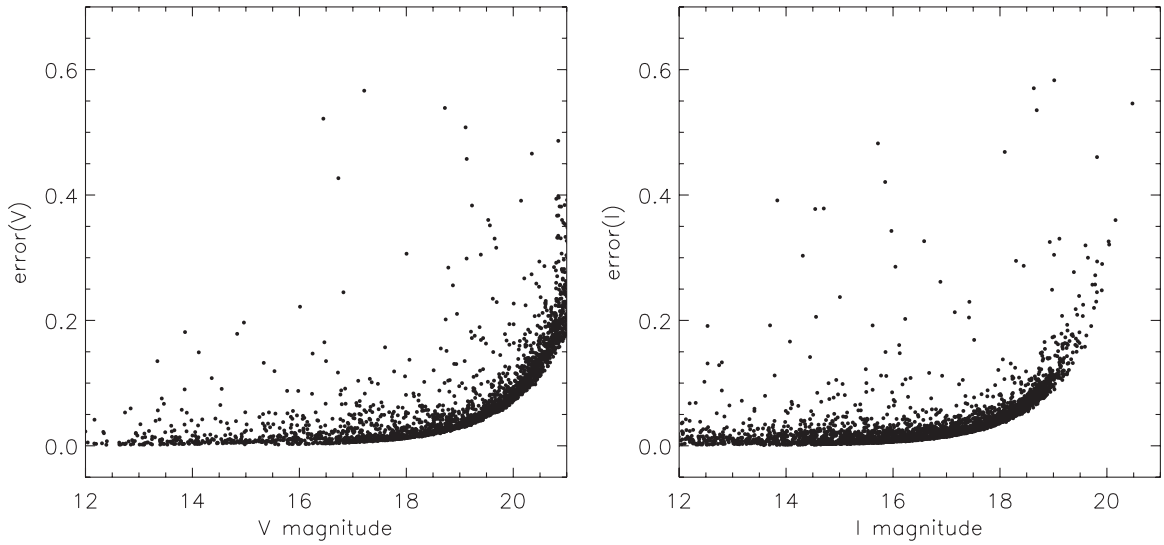

Figure 3. Errors in V (left) and I (right) band photometry. The errors shown here are the greater of the IRAF calculated error and the median absolute deviation.

the short exposure is used for the photometry. Measurements that are affected by bleeding or crosstalk from a saturated star are manually removed. Finally, we combine all the photometry measurements for the same star by taking the median value.

To estimate the photometric error, we use both the error estimated by the IRAF *phot* and the variation in separate observations of the same star. The IRAF *phot* package only takes into account Poisson statistics, which tends to underestimate the true uncertainty. To provide a better estimate of our errors, we take the stars for which we have at least four long-exposure measurements to find the median absolute deviation (MAD), a robust measure of the deviation. Since most fields are observed on both nights and the measurements from both nights are used, the deviation implicitly takes into account of potential effects due to variable atmospheric extinction and seeing from one night to another. If a star is saturated in the long exposures, then the short-exposure measurements (in the case where there are more than two short exposures) are used. We estimate the photometric error for each star from the greater of the *phot* calculated error and the MAD. The results are shown in Figure 3. The typical errors are less than 0.05 mag for stars brighter than $V = 19$ or $I = 18$. This error is comparable to the errors obtained in the calibration of Landolt stars and is most likely due to the non-photometric weather conditions. The typical error then increases drastically with fainter stars due to uncertainties in photon statistics. A small fraction of stars have errors much larger than the typical errors, which can be due to non-photometric conditions (cirrus in the beginning of the night), as well as intrinsic variability of the stars from one night to another. We think intrinsic variability contributes to the measured errors because we examined the list of stars with the largest errors and many of them turned out to be known variable stars.

We were able to obtain photometry of stars with V and I magnitude between 12 and 22 mag. However, from Figure 3, we know that the typical error of a $V = 21$ mag star is about 0.2 mag and the error increases rapidly for fainter objects. We therefore limit our photometric sample to stars with V magnitudes between 12.5 and 21, I magnitudes between 12 and 20.5, and $V - I$ between 0.5 and 4 mag with the typical error of a 21 mag star being 0.2 mag.

Figure 4 shows the V versus $V - I$ color–magnitude diagram (CMD) of the sample mentioned above. The top panel shows

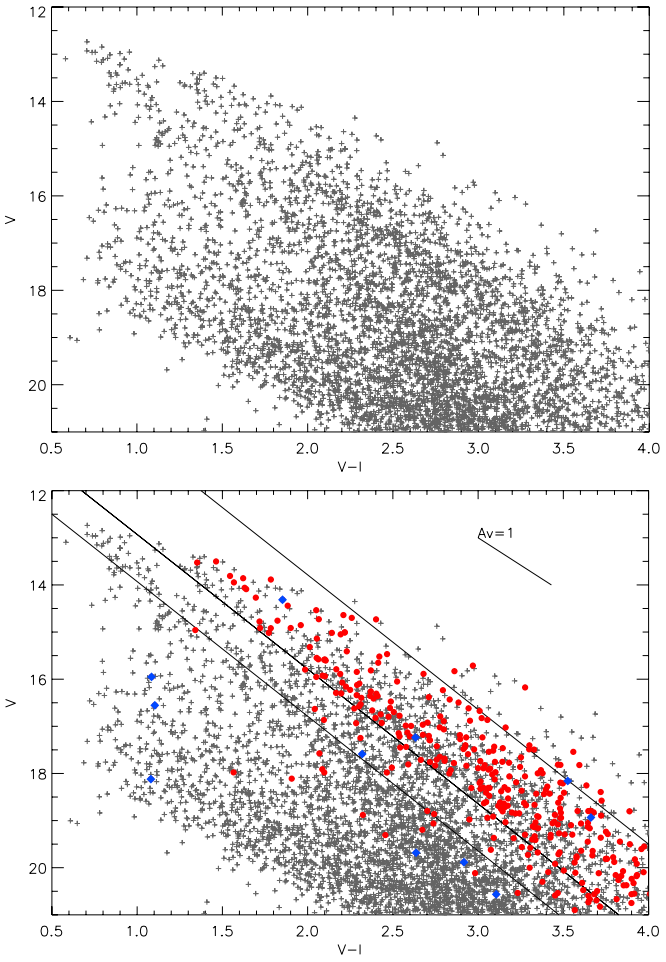

Figure 4. Top: V vs. $V - I$ color–magnitude diagram of objects in L1641, showing all the photometric data. Bottom: same figure, with protostars (blue diamonds) and disk objects (red circles) overplotted. The YSOs with disks (red circles) lie mostly in a small region of the CMD, marking the region populated by the pre-main-sequence stars. There are 772 non-IR-excess sources (gray crosses) in the same region of the CMD. This photometry was taken in 2010 December with OSMOS on the MDM 2.4 m telescope. The extinction vector is the standard extinction taken from Cardelli et al. (1989) with $R_v = 3.1$. The parallel lines are discussed in Section 4.1.

(A color version of this figure is available in the online journal.)

all the stars in our sample, regardless of its IR excess, and the bottom panel shows the same plot, with the Class I protostars shown in blue diamonds and the Class II stars (IR-excess objects with disks) shown in red circles.

We note that most of the Class II stars in Figure 4 fall in a small region on the CMD, which we approximate with the top two parallel lines. The bottom of the young stellar object (YSO) region is traced by a line through the two points $(V - I, V) = (0.5, 11.5)$ and $(4, 21.5)$, and the top is 2 mag above it in V at a given $V - I$. We expect that the Class III stars (pre-main-sequence objects with no IR excess) have similar ages and distances and therefore fall in the same region of the CMD. However, not all the non-IR-excess objects in this region are members. We therefore target them in our optical spectroscopy surveys to confirm their membership.

2.2. Optical Spectra

There are two parts to our optical spectroscopic sample. The first part is the sample of infrared-excess stars from the *Spitzer* survey of S. T. Megeath et al. (2012, in preparation). Figure 1 shows fields covered by the *Spitzer* survey and the positions of the IR-excess stars. The *Spitzer* survey identified 166 protostars and 723 disk objects in L1641 (defined as the field outlined in Figure 1 but stopping at -6°). Note that only 8% of the protostars and 48% of the disk objects are found in our optical photometric sample and are therefore sufficiently bright for optical spectroscopy. The second part of our sample is non-IR-excess objects selected based on their optical photometry. There are a total of 772 non-excess stars that satisfy the optical photometry selection, and we were able to target 95% of these objects in our spectroscopy. The sample is, however, biased against heavily reddened objects.

The spectra were obtained with multi-aperture spectrographs covering extended fields of view. Approximately 75% of our spectra were obtained with Hectospec, the fiber-fed multiobject spectrograph on the 6.5 m MMT on Mt. Hopkins (Fabricant et al. 2005). It has 300 fibers that can be placed within a 1° diameter field. Each Hectospec fiber subtends $1\farcs5$ on the sky. The observations were taken with 270 line mm^{-1} grating, providing ~6.2 Å resolution and spectral coverage of 3650–9200 Å. With 17 observations from 2006 to 2011, a total of 2369 stars were observed. The total on-target exposure times are 45–50 minutes for most fields, with the exception that the 2009 January 30 field was observed for 22.5 minutes. The top panel of Figure 5 shows fields of the Hectospec observations. Targets for observing runs from 2006 to 2009 are selected based on their IR colors (fields shown in blue), and the targets of the 2011 run are selected based on their optical photometry (fields shown in magenta, see Section 2.1 for selection criteria). We first maximized the number of targets that satisfy either the IR excess or optical selection criteria and then filled in the remaining fiber positions with other stars in the field.

The Hectospec data were reduced through the standard Hectospec data reduction pipeline (Mink et al. 2007), except for sky background subtraction. The pipeline assumes that the sky background does not vary significantly with position on the sky and uses "sky fibers," or fibers that point to empty portions of the sky, to correct for the sky background. However, in a star-forming region, nebulosity may result in significantly varying sky background and therefore bad estimates of nebular lines. Our sky subtraction takes into account the spatial variations of the sky background. Some of the observations were taken along with offset sky spectra, $5''$ apart from the star, in which case we

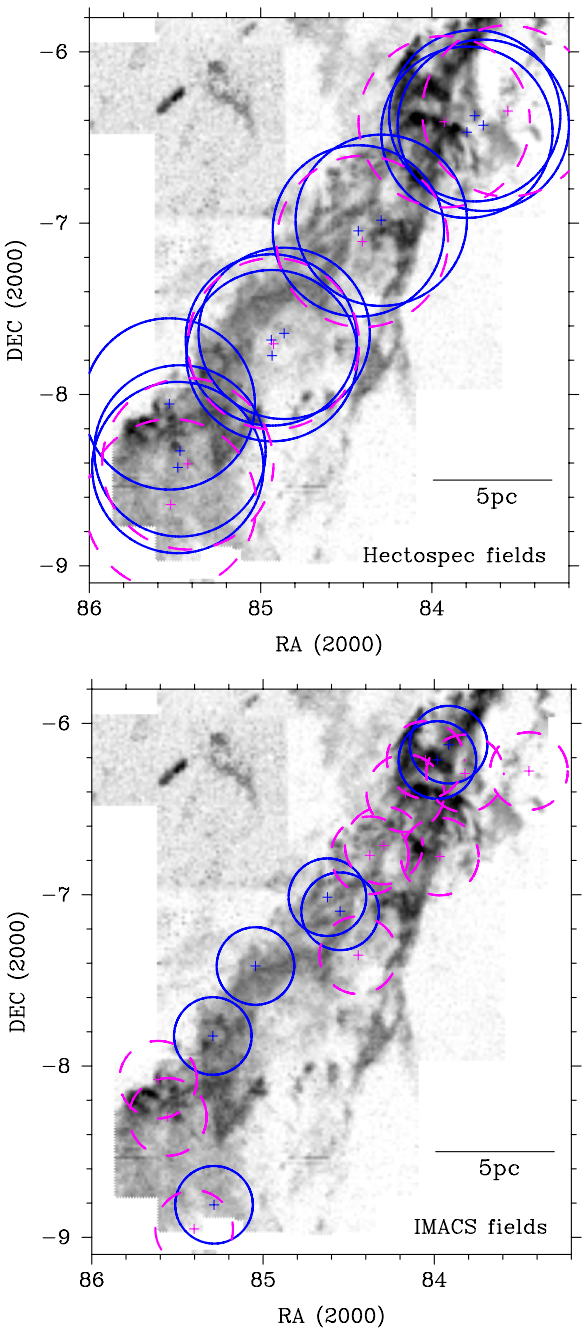

Figure 5. Optical spectroscopy fields overlaid on the ^{13}CO map from Bally et al. (1987). The Hectospec fields (top) are chosen to maximize the number of IR-excess objects observed. The IMACS fields (bottom) are either IR-selected (blue solid circles) or optical-selected (magenta dashed circles). The IMACS fields are mainly used to compliment the Hectospec fields in crowded regions. The physical scale of 5 pc is also shown in the plot, assuming a distance of 420 pc.

(A color version of this figure is available in the online journal.)

subtracted the offset sky spectra from the science target spectra. When the offset sky spectra were not taken, we used the closest 3–5 sky fibers as the average sky and subtracted it from the science spectra. We tested our sky subtraction methods with sky fibers (so a perfect sky subtraction would leave a spectrum with only noises around 0) and found that the quality of the resulting spectra is significantly improved with the offset sky spectra, with most of the Hα emission and other sky lines accounted for, whereas the nearest 3–5 sky fibers improve the overall sky

subtraction (especially night-sky emission lines in the near-IR) but do not correct for the nebular lines very well.

Another 25% of our spectra were obtained with IMACS, the Inamori–Magellan Areal Camera & Spectrograph on the Magellan Baade telescope (Bigelow & Dressler 2003). We used the IMACS $f/2$ camera in multi-slit spectroscopy mode with the 300 line grism at a blaze angle of 17.°5. With a 0.″6 slit, this configuration yields a resolution of 4 Å and spectral coverage of approximately 4000–9000 Å (stars close to the edge of the fields may not have full spectral coverage). From 17 observations in 2010 and 2011, a total of 715 stars were observed. The standard observation time for each field is 5 × 10 minutes, but we increased the time to 6 × 10 minutes for a few observations at higher airmasses. The bottom panel of Figure 5 shows the fields of the IMACS observations. The targets of the first IMACS run were selected based on their IR colors (shown in blue), and the targets of the second run are selected based on their optical photometry (shown in magenta; see Section 2.1 for selection criteria). The IMACS data were reduced with COSMOS, the Carnegie Observatories System for MultiObject Spectroscopy, following the standard cookbook.

Under good observing conditions, we were able to spectral-type stars as faint as $V \sim 21$. However, the faintest magnitude we can spectral-type depends on the seeing and the instrument used.

3. RESULTS

3.1. Photometry

Figure 4 shows the V versus $V - I$ CMD of the stars between $V - I \sim 0.5$–4 and $V < 21$. There are a total of 4475 stars in this photometric sample. Correlating the optical photometry and the IR-excess classification (Gutermuth et al. 2009), we mark the IR-excess objects in our photometry (bottom panel). Thirteen of the stars were protostars (blue diamonds), and 347 of them were YSOs with disks (red circles). Compared to the number of IR-excess objects identified in the *Spitzer* survey, only 8% of the protostars and 48% of the disk objects are found in our photometric sample. The optical photometry fields cover slightly less area than the *Spitzer* survey but cover 95% of the IR-excess objects. It is not surprising that we do not find most of the protostars as they are highly embedded in their envelopes. We were only able to identify half of the stars with disk excesses in the optical photometry due to extinction (see Section 3.4).

3.2. Spectra and Spectral Types

Figures 6 and 7 show some example spectra of confirmed members from Hectospec and IMACS, respectively, arranged by their spectral types. The Hα equivalent width criteria by White & Basri (2003) are used to determine whether they are classical T Tauri stars (CTTS) or weak-line T Tauri stars (WTTS). Note that IMACS has very little transmission in the blue whereas the transmission of Hectospec is more uniform across the spectral range. The [O I] line at 5577 Å is very prominent in some Hectospec data but is actually a sky line that was not correctly subtracted. In this case, the Hα emission is also likely affected by bad sky subtraction. Figure 8 show IMACS spectra of rapidly accreting stars. They have not only a high Hα equivalent width but also other emission lines such as [O I], He I, and the infrared Ca triplet. The last two spectra have particularly high Hα equivalent widths and show O I emission at 7773 Å and the higher orders of the Paschen series.

We determine the spectral types of our Hectospec and IMACS data with SPTCLASS, a semi-automatic spectral-typing program (Hernández et al. 2004). It uses empirical relations of spectral type and equivalent widths to classify stars. It has three schemes optimized for different mass ranges (K5 or later, late F to early K, and F5 or earlier), which use different sets of lines. The user has to manually choose the best scheme for each star based on the prominent features in the spectrum and the consistency of several indicators. While SPTCLASS is insensitive to reddening and signal-to-noise ratio (S/N) of the spectra (as long as one can obtain a good flux estimate), it does not take into account the effect of the hot continuum emission produced by the accretion shocks. This continuum emission makes the photospheric absorption lines appear weaker. SPTCLASS generally assigns an earlier spectral type to veiled stars and therefore the SPTCLASS outputs should be considered as the earliest spectral-type limits. Highly veiled stars (such as the ones shown in Figure 8) are not spectral-typed. Eight of our program stars are too veiled for spectral typing.

We also complement our results with data from Fang et al. (2009, hereafter F09), which include spectral-type estimates and Hα and Li I equivalent widths for 266 stars. The majority of the spectral types come from their VLT/VIMOS observations, and some are from Gâlfalk & Olofsson (2008) and Allen (1995). We observed 206 of the stars in the F09 sample; Figure 9 compares our spectral types with theirs. Since the spectral types in F09 come from multiple sources, we use different symbols to indicate the source. Most of the spectral types are consistent within two subclasses, and there is no systematic trend in the differences; the only major large inconsistency is for a rapidly accreting G-type star, which has an uncertain spectral type because of very high veiling. For consistency we therefore use the spectral type from our observations for the objects in common and incorporate the data from F09 for the stars we did not observe.

Figure 10 shows the distribution of spectral types of confirmed members. The distribution peaks around M4; we are systematically incomplete in the later-type population because of extinction (see Section 3.4). Due to the magnitude criteria in our target selection, there are very few stars earlier than K in our sample. We will address this in a forthcoming paper, where we attempt to identify the intermediate-mass members.

We use the following criteria to identify young stars in our sample:

(1) We include all IR-excess stars using *Spitzer*/IRAC and 2MASS *JHK* colors (the IR-excess selection criteria can be found in Gutermuth et al. 2009; the complete catalog will be published in S. T. Megeath et al. 2012, in preparation). For all non-IR-excess stars, we identify them as members if (2) Li absorption at 6707 Å is clearly detectable and has an equivalent width consistent with youth (the EW(Li) has to be greater than the Pleiades value for the same spectral type from Briceno et al. 1997) or (3) Hα emission is clearly above the background nebulosity.

Criterion (2) is reliable in selecting pre-main-sequence M and late K stars, but for early K and G stars it can be more problematic, as Li depletion timescales can be quite long (see, e.g., discussion in Briceno et al. 1997). Thus, to identify G and early K members, we require that the equivalent widths of Li absorption lines be greater than that observed in Pleiades (Briceno et al. 1997) or the Hα equivalent widths in emission

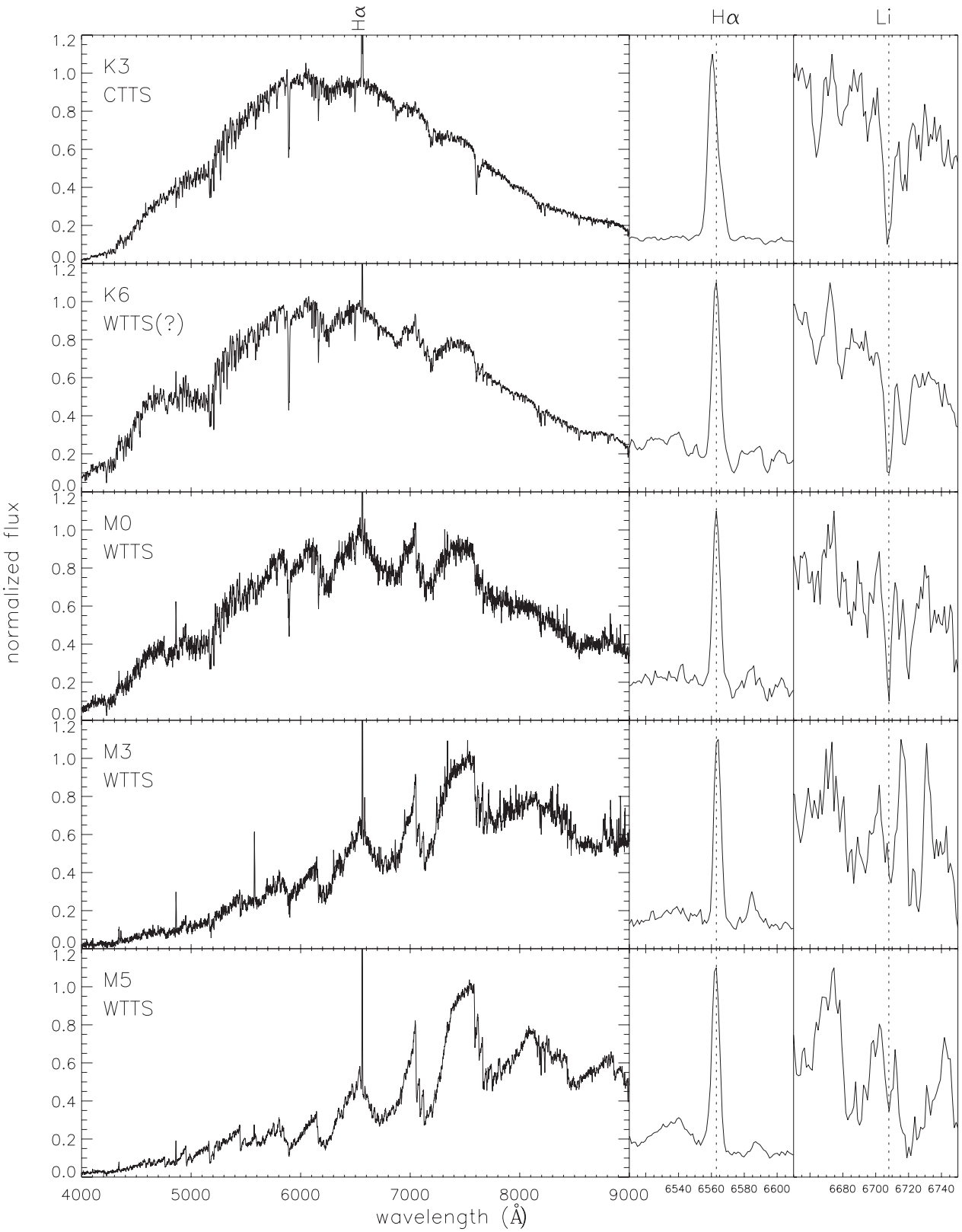

Figure 6. Examples of spectra from Hectospec with a zoom-in view around Hα (λ6563) and Li I (λ6707). From top to bottom, the spectra are spectral-typed: K3, K6, M0, M3, and M5. The [O I] line at λ5577 is a prominent sky line. The red end of the M-type spectra is affected by series of sky lines. Their TTS type is classified using the definition given by White & Basri (2003). The Hα equivalent width in the K6 star is bordering the cutoff in the definition.

or filled in above the expected absorption equivalent widths (Stauffer et al. 1997).

Whether or not the observed Hα emission—criterion (3)—is actually from the star or simply nebular emission can be difficult to distinguish in some regions and especially for faint stars. We therefore compiled two lists of objects, one with only confirmed members of L1641 and one with potential members but having a higher contamination rate.

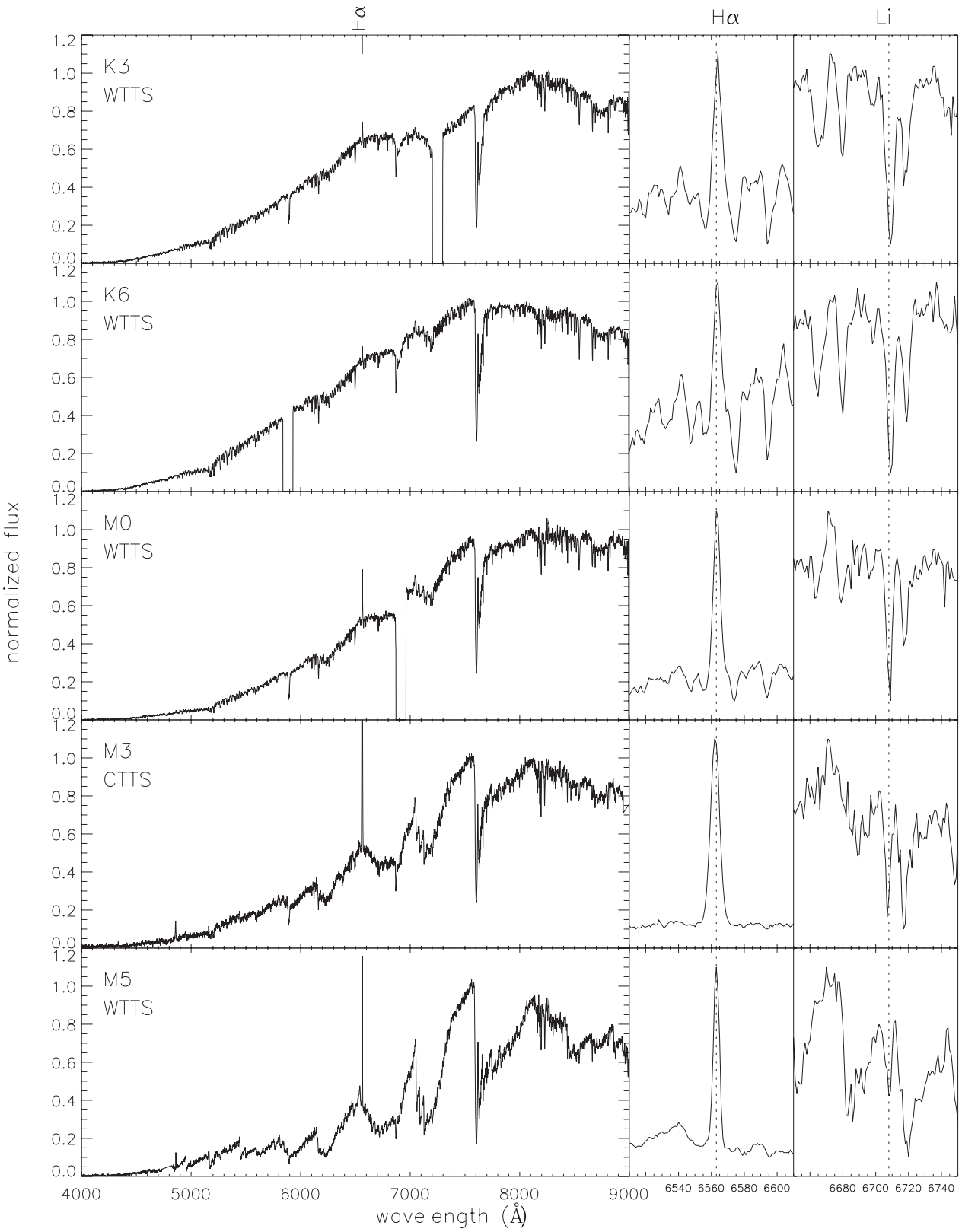

Figure 7. Examples of spectra from IMACS with a zoom-in view around Hα (λ6563) and Li I (λ6707). From top to bottom, the spectra are spectral-typed: K3, K6, M0, M3, and M5.

To ensure a self-consistent sample, we extracted members from the F09 sample using the same criteria used in our own spectra; therefore, not all the members listed in F09 are included in our results here. In total, we adopted the F09 data for 41 stars that were not targeted in our observations; five of them are considered "probable members" due to the lack of Li absorption data.

Table 1 lists the number of confirmed members (including IR-excess members and non-excess members) and probable members from the three sources (Hectospec, IMACS, and F09).

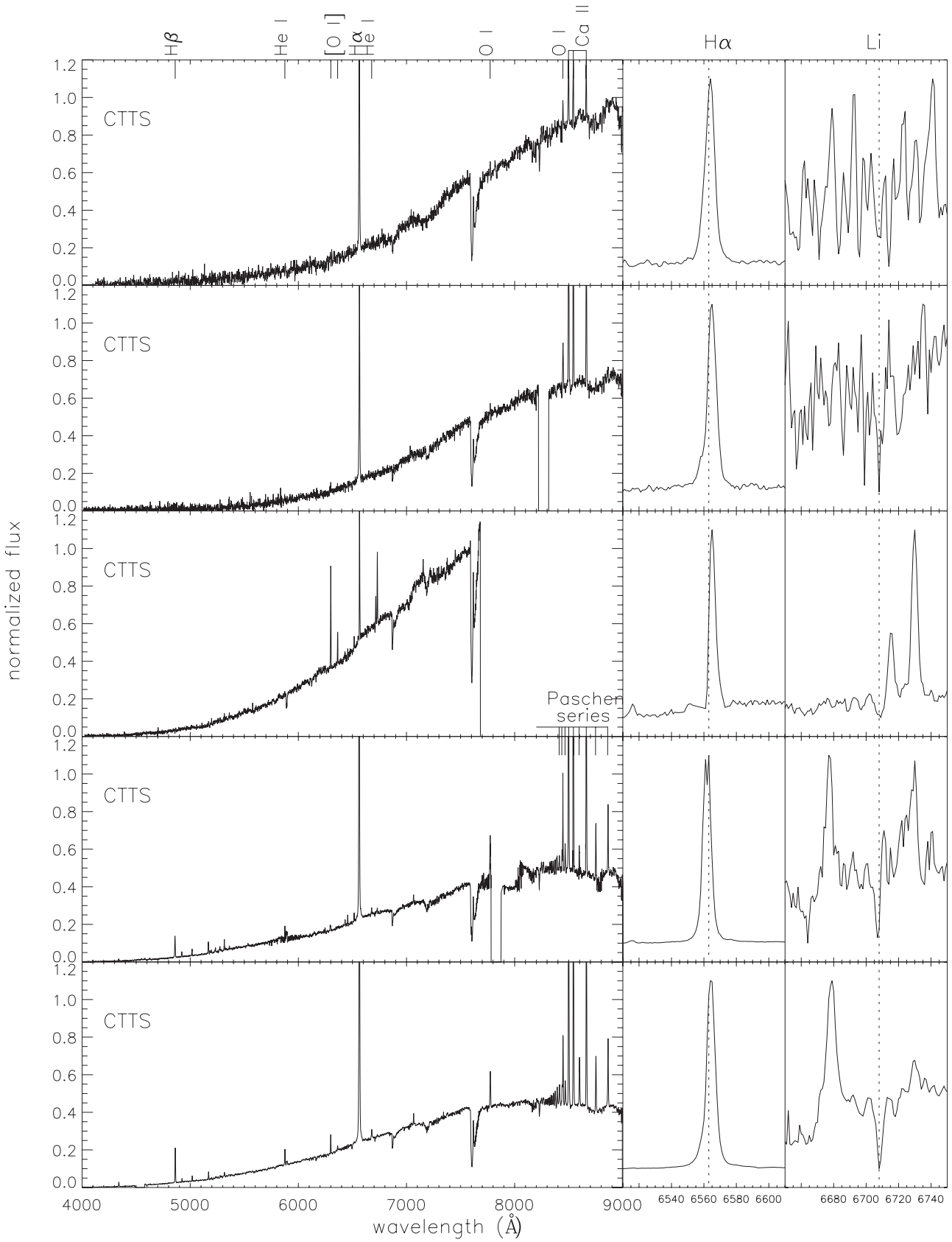

Figure 8. Example IMACS spectra of rapid accretors with a zoom-in view around Hα (λ6563) and Li I (λ6707). The spectra are highly veiled and therefore make spectral typing difficult. The main emission lines have been marked.

Table 2 gives the positions, photometry, spectral types, etc., of the 864 confirmed members, confirmed by either their IR excess or unambiguous Li absorption. Out of the 864 confirmed members, 406 of them have IR excess, while 458 have no excess. Eight of the confirmed members are highly veiled by excess continuum emission, thought to be produced by the accretion

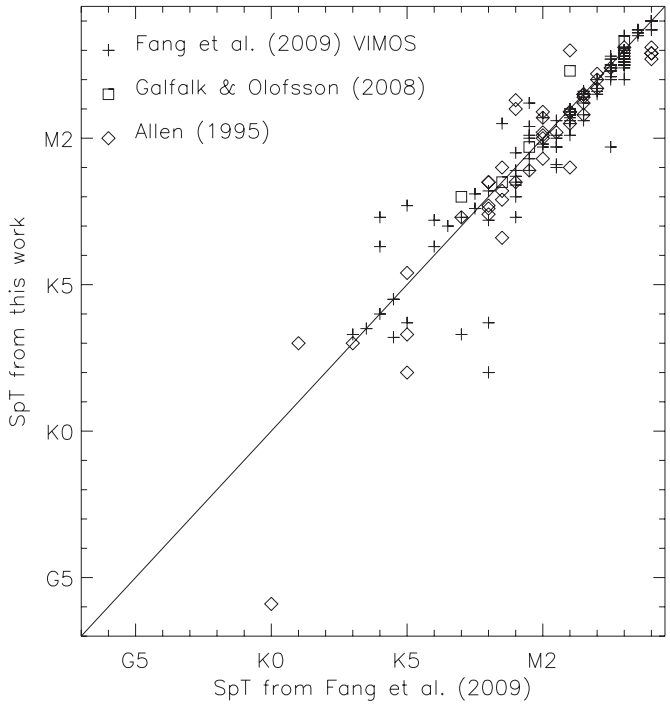

Figure 9. Comparison of the spectral types obtained by Fang et al. (2009) and this work for the 166 objects that are included in both samples. The catalog of Fang et al. (2009) comes from three sources: (1) their VLT/VIMOS observations (crosses), (2) Galfalk & Olofsson (2008, squares), and (3) Allen (1995, diamonds). The highly discrepant star near the bottom is heavily veiled (see the text).

Table 1
Spectroscopic Members

Source	Confirmed Members	IR Excess	No IR Excess	Probable	Total
Hectospec	517	235	282	69	586
IMACS	311	142	169	24	335
Fang09[a]	36	29	7	5	41
Total	864	406	458	98	962

Note. [a] Fang et al. (2009) cataloged 266 stars in L1641. The numbers here show only stars we did not observe.

shock on the stellar photosphere (Koenigl 1991). Spectral typing is not possible for these objects.

Table 3 gives the positions, photometry, spectral types, etc., of the 98 probable members. The probable members are stars that show Hα emission and are in the strip of V versus $V-I$ CMD (see bottom panel of Figure 4) that most of the confirmed YSOs reside in. They do not, however, have IR excess or unambiguous Li absorption line (most likely due to low S/N of the spectra). We therefore catalog them as probable members. These probable members are excluded in our analysis and statistics unless otherwise noted.

The top panel of Figure 11 shows the positions of spectroscopically confirmed members overplotted on the ^{13}CO map from Bally et al. (1987). The distribution of the spectroscopic members in general follows the gas distribution. The bottom panel shows the positions of probable members. Probable members that are located near the group of confirmed members are more likely members, whereas the ones far away from any confirmed members are likely non-members with nebular Hα emission.

Figure 12 shows the spectroscopically confirmed members on the CMD color-coded by their spectral types. It shows that we can spectral-type objects down to M5–M6 as long as they

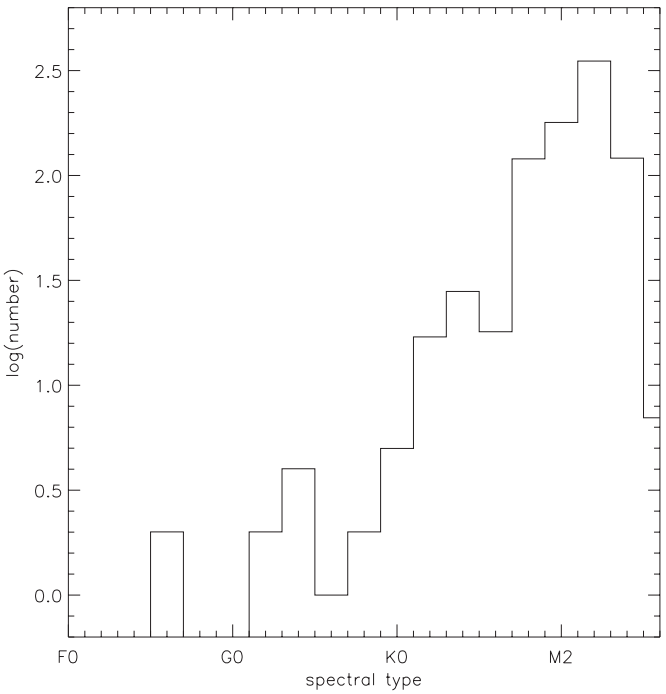

Figure 10. Distribution of spectral types of all confirmed members with spectral-type information from Table 2. Due to the magnitude criteria in our target selection, there are missing stars earlier than K in our sample.

are not highly extincted (in general, $A_V < 2$). There are some objects well below the YSO regions, most of which are IR-excess objects. Most likely they are edge-on disk objects that are seen in scattered light and therefore appear much bluer than typical YSOs. This figure also shows that the magnitude limits of our optical photometry and spectroscopy are well matched.

The solid lines in Figure 12, from top to bottom, are the Siess et al. (2000) isochrones for 1, 2, 3, and 4 Myr. Because the isochrones are almost parallel to the reddening vector, we can use the non-extinction-corrected CMD to estimate the age of the population. Most of the population lies within the 1 Myr and 4 Myr isochrone, and the distribution peaks around 3–4 Myr. Using the Siess isochrones, Da Rio et al. (2010) found the age of the ONC to be ~2–3 Myr. The L1641 population, on average, thus appears to be slightly older than the ONC population, even though the age difference is comparable to the age uncertainties. This means that ultimately we should be able to make a direct comparison for IMFs using spectral types without correction.

3.3. Hα as a Membership Indicator and Accretion Diagnostics

The optical spectra also provide us with diagnostics of accretion. Tables 2 and 3 list equivalent widths of Hα, which can be used as an indicator of accretion as the Hα luminosity correlates with the accretion luminosity. Fang et al. (2009) have an extensive discussion on accretion rates and disk properties in selected areas of L1641 using Hα, Hβ, and He I λ5876.

Table 4 lists other accretion indicator emission lines we found in the spectra. Note that if an emission line is not listed, it does not necessarily mean there is no emission line, but rather we cannot confidently tell that there is an emission line due to sky subtraction issues or limited spectral coverage in some IMACS data.

Figure 13 shows Hα equivalent widths of all confirmed members versus spectral type. The Hα equivalent widths can be used as an indicator of accretion as the Hα luminosity correlates

Table 2
Confirmed Members in L1641

ID	R.A. (J2000)	Decl. (J2000)	V (mag)	I (mag)	J[a] (mag)	H[a] (mag)	K_S[a] (mag)	Spectral Type	IR Excess[b]	EW(Hα) (Å)	EW(Li) (Å)	Date Observed[c]
1	83.21121	−6.18593	17.430	14.793	13.450	12.740	12.537	M3.0 ± 0.6[d]	N	−4.30	0.4	2011 Oct 22
2	83.22298	−6.10026	17.670	14.743	13.146	12.499	12.259	M3.6 ± 0.6[d]	N	−11.0	0.4	2011 Oct 22
3	83.23454	−6.05524	16.566	14.356	13.040	12.405	12.235	M1.5 ± 0.7[d]	N	−6.00	0.5	2011 Oct 22
4	83.24131	−6.04519	16.819	14.377	12.975	12.324	12.117	M2.6 ± 0.5[d]	N	−4.00	0.3	2011 Oct 22
5	83.30244	−6.05771	17.607	14.925	13.508	12.879	12.632	M3.0 ± 0.6[d]	N	−4.20	0.3	2011 Oct 22
6	83.30896	−6.19689	17.006	14.462	13.006	12.329	12.074	M2.6 ± 0.5[d]	N	−22.6	0.3	2011 Oct 22
7	83.31703	−6.30980	15.290	13.320	12.061	11.383	11.151	M0.5 ± 0.5[d]	N	−3.60	0.5	2011 Oct 22
8	83.33062	−6.24046	17.858	14.796	13.158	12.535	12.274	M4.6 ± 0.6[e]	N	−7.90	0.3	2011 Oct 11
9	83.33256	−6.07309	16.396	14.081	12.722	12.013	11.826	M2.2 ± 0.6[d]	Y	−5.90	0.4	2011 Oct 22
10	83.34235	−6.19836	15.604	13.608	12.415	11.724	11.530	M0.6 ± 0.5[e]	N	−3.20	0.5	2011 Oct 11

Notes.
[a] J, H, K_S photometry is from 2MASS.
[b] Criteria for IR excess are defined in Gutermuth et al. (2009) and S. T. Megeath et al. (2012, in preparation).
[c] Local date at the beginning of the night.
[d] Data from Hectospec spectra.
[e] Data from IMACS spectra.
[f] Data from Fang et al. (2009). No spectral-typing error estimate.

(This table is available in its entirety in a machine-readable form in the online journal. A portion is shown here for guidance regarding its form and content.)

Table 3
Probable Members in L1641

ID	R.A. (J2000)	Decl. (J2000)	V (mag)	I (mag)	J[a] (mag)	H[a] (mag)	K_S[a] (mag)	Spectral Type	IR Excess[b]	EW(Hα) (Å)	EW(Li) (Å)	Date Observed[c]
1	83.31244	−6.19215	18.897	15.697	14.001	13.429	13.142	M4.6 ± 0.7[d]	N	−9.40	···	2011 Oct 11
2	83.33856	−6.01960	19.102	15.608	13.731	13.171	12.890	M4.6 ± 1.0[e]	N	−11.6	···	2011 Oct 22
3	83.35003	−6.11952	16.900	14.259	12.708	12.051	11.804	M3.2 ± 1.1[e]	N	−11.3	···	2006 Nov 20
4	83.37934	−6.39085	18.752	15.434	13.776	13.197	12.927	M5.0 ± 0.7[d]	N	−12.7	···	2011 Oct 11
5	83.42722	−6.05974	19.915	16.364	14.475	13.786	13.501	M4.5 ± 1.0[e]	N	−6.40	···	2011 Oct 22
6	83.54100	−6.38943	17.206	14.619	13.204	12.576	12.333	M3.1 ± 0.5[e]	N	−6.90	···	2011 Oct 22
7	83.55022	−6.28399	18.653	15.151	13.345	12.711	12.427	M5.0 ± 0.7[d]	N	−9.70	···	2011 Oct 11
8	83.56502	−6.40473	19.209	15.796	13.950	13.362	13.053	M4.0 ± 1.0[e]	N	−5.70	···	2011 Oct 22
9	83.63090	−6.03181	19.917	16.230	14.216	13.575	13.287	M5.1 ± 0.8[e]	N	−8.70	···	2006 Nov 20
10	83.64370	−6.07540	19.709	16.125	14.116	13.593	13.246	M5.0 ± 2.0[e]	N	−8.70	···	2011 Oct 22

Notes.
[a] J, H, K_S photometry is from 2MASS.
[b] Criteria for IR excess are defined in Gutermuth et al. (2009) and S. T. Megeath et al. (2012, in preparation).
[c] Local date at the beginning of the night.
[d] Data from IMACS spectra.
[e] Data from Hectospec spectra.
[f] Data from Fang et al. (2009). No spectral-typing error estimate.

(This table is available in its entirety in a machine-readable form in the online journal. A portion is shown here for guidance regarding its form and content.)

Table 4
YSOs with Strong Emission Lines

ID	R.A. (J2000)	Decl. (J2000)	[O I] λ5577	[O I] λ6300	[O I] λ6363	[N II] λ6548	[N II] λ6583	He I λ6678	[S II] λ6716	[S II] λ6731	[O I] λ7773	[O I] λ8446	[Ca II] λ8498	[Ca II] λ8542	[Ca II] λ8662
6	83.30896	−6.19689	···	···	···	···	···	···	···	···	···	···	−0.56	−0.27	−0.12
9	83.33256	−6.07309	···	−2.0	−0.37	···	···	···	···	···	···	···	···	···	···
13	83.35634	−6.10948	···	−5.5	−1.4	···	−0.40	−1.4	···	···	−0.70	−1.9	−6.8	−6.5	−5.8
20	83.38751	−6.31044	−4.7	−81.	−27.	···	−7.7	−1.1	−5.6	−8.7	−1.0	−5.6	−15.	−16.	−13.
29	83.42479	−6.26354	···	−4.8	···	···	···	−2.2	···	···	···	−6.4	−5.7	−6.3	−5.2
34	83.43911	−6.07385	···	−0.49	···	···	···	−1.8	···	···	−1.0	−1.8	−20.	−22.	−18.
38	83.45954	−6.36361	···	−2.7	−0.70	···	−1.5	···	−0.16	−0.47	···	···	···	···	···
64	83.57055	−6.54707	···	−4.7	−1.2	···	···	···	···	···	···	···	···	···	···
89	83.65066	−6.09297	···	−0.75	−0.13	···	···	−1.4	···	···	−0.59	−1.4	−2.0	−2.1	−2.0
91	83.65124	−6.27344	···	−1.3	···	···	···	−2.2	···	···	···	···	···	···	···

(This table is available in its entirety in a machine-readable form in the online journal. A portion is shown here for guidance regarding its form and content.)

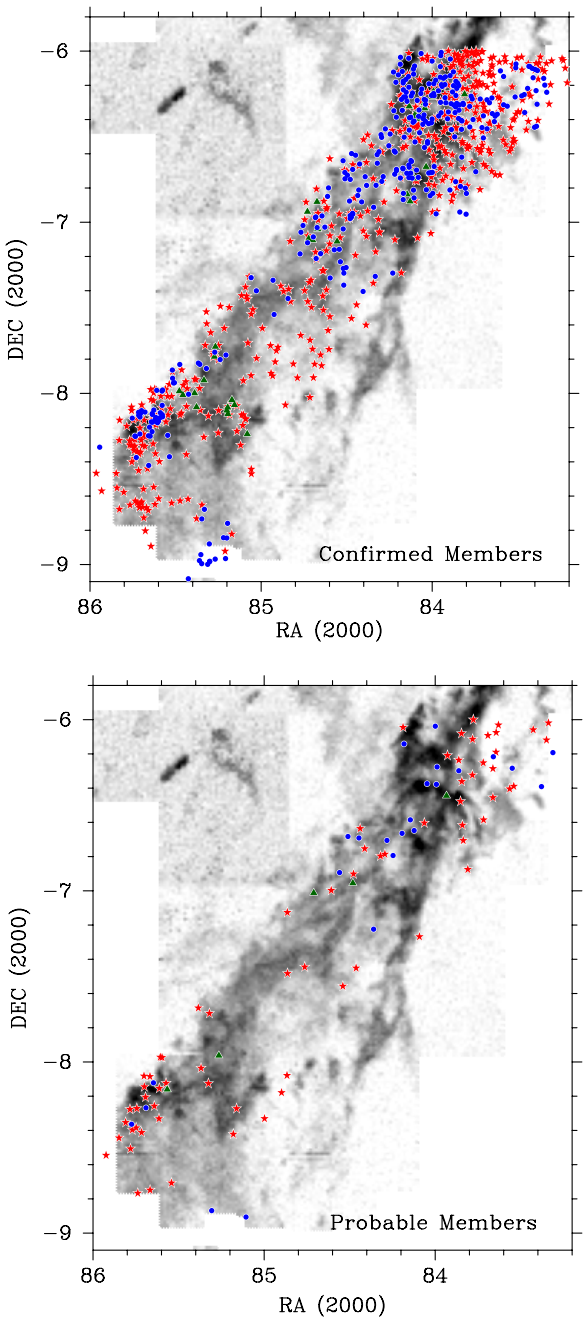

Figure 11. Top: positions of spectroscopically confirmed members in Table 2 overplotted on the ^{13}CO map from Bally et al. (1987). The symbols indicate the sources of the spectra. Red stars and blue circles represent objects observed with Hectospec and IMACS, respectively. Green triangles represent spectral types taken from F09. Bottom: positions of probable members in Table 3.

(A color version of this figure is available in the online journal.)

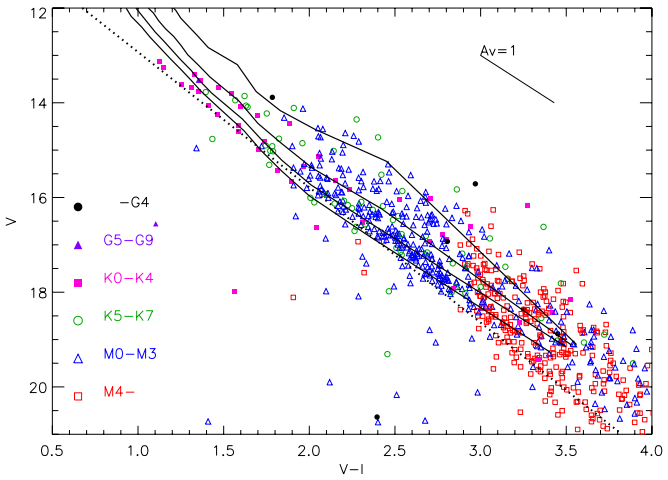

Figure 12. Spectroscopically confirmed members on the CMD color-coded by their spectral types (not corrected for extinction). The solid lines are 1, 2, 3, and 4 Myr isochrones from Siess et al. (2000) (from top to bottom), and the dotted line is the line used to define the YSO region. The minimum mass of the plotted isochrones is 0.1 $M_{\odot}$.

(A color version of this figure is available in the online journal.)

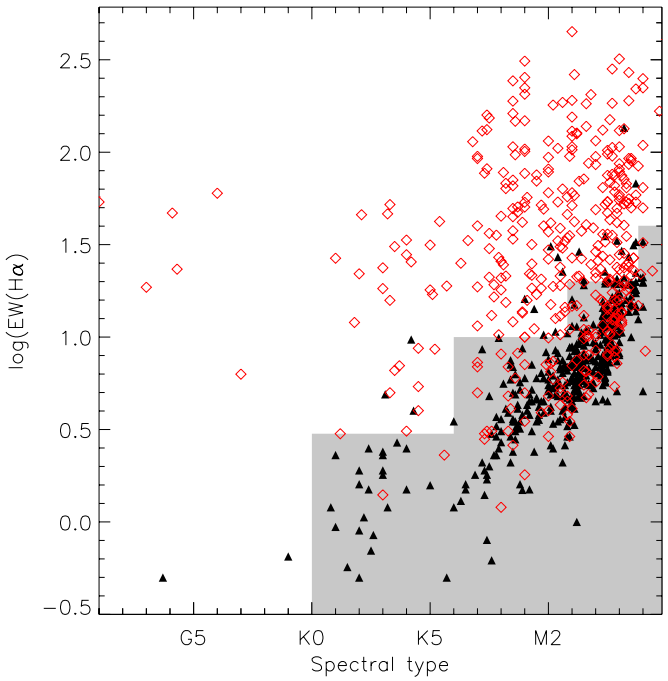

Figure 13. Hα equivalent widths (in log scale) of all confirmed members vs. spectral type. The red open diamonds are IR-excess members, and black filled triangles are non-IR-excess members. The shaded region shows where the WTTS objects reside using CTTS/WTTS classification from White & Basri (2003). Note that this classification only applies to stars later than K0.

(A color version of this figure is available in the online journal.)

with the accretion luminosity. In general, the Hα equivalent widths have an increasing trend toward later spectral types and the IR-excess objects (red open diamonds) have higher Hα equivalent widths than the non-excess objects (black solid triangles). The shaded region shows the Hα equivalent width criteria for CTTS and WTTS by White & Basri (2003). Using these T Tauri criteria, 299 of the confirmed are CTTS and 565 are WTTS, which gives a CTTS/ WTTS ratio of 53%. In the early K to G spectral-type range, there are a few stars with very low EW(Hα) equivalent widths.

We now look at the stars with very low Hα equivalent widths in more detail. The top panel of Figure 14 shows the Hα equivalent widths versus spectral type for objects with Hα equivalent widths less than 1 Å in emission. Note that in this plot emission is positive and that the y-axis is in linear scale. The dashed line shows the Hα equivalent widths measured in the Pleiades from chromospheric activity (Stauffer et al. 1997). We note that four of the members fall on or below the dashed line. The bottom panel of Figure 14 shows the Li equivalent widths of the same stars, where the stars with particularly low

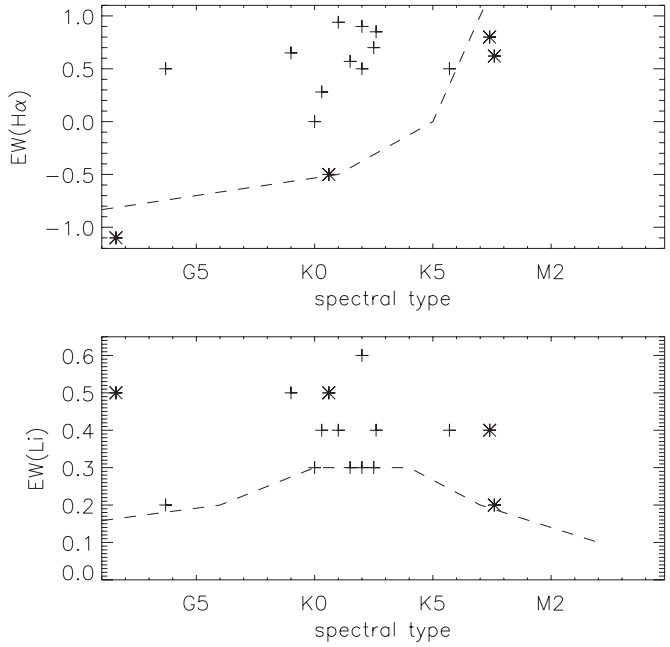

Figure 14. Top: Hα equivalent widths (in linear scale) of objects with Hα equivalent widths less than 1 Å in emission. The dashed line is the approximate relation for chromospheric activity in the Pleiades (Stauffer et al. 1997). Note that here emission in Hα is defined as positive equivalent width, consistent with Figure 13, but different from Table 2. Bottom: equivalent widths of Li absorption for the same objects. Absorption in Li is defined as positive equivalent width. The dashed line shows the approximate relation for the maximum Li absorption in the Pleiades for a given spectral type (Briceno et al. 1997).

Hα are shown in asterisks. All the low Hα stars shown in the top panel show Li absorption above the Pleiades level (Briceno et al. 1997) and are listed as confirmed members. Although it is possible that some of these objects are from previous star-forming events in the Orion complex and still show Hα and Li, the number of low Hα objects is very small and has little effect on our overall sample.

3.4. Extinction

We use the color excess $E(V-I)$ to estimate the extinction toward a star. For stars earlier than M4, we use the main-sequence colors from Kenyon & Hartmann (1995); for stars M4 and later, we use the intrinsic colors of the young disk population described by Leggett (1992). We then calculate the extinction assuming a standard extinction law with R_V of 3.1 (Cardelli et al. 1989). The $E(V-I)$ method has certain limitations and uncertainties. For example, Da Rio et al. (2010) have shown that accretion onto a star makes it look bluer and therefore the extinction would be underestimated.

Figure 15 shows the distribution of extinction versus spectral type. 80% of our spectral-typed members have $A_V \leqslant 2$. On average, the IR-excess objects (open red diamonds) appear to have higher extinction than the non-excess objects, which is partially a selection effect because we are unable to identify non-excess members through Li absorption in high-A_V regions where the S/N is much lower for the same spectral type. Negative values of A_V are non-physical and are due to errors in spectral types, photometry, and also uncertainties in their intrinsic colors. Since the spectral-typing errors and photometric errors are larger for the faintest objects, it makes sense to see more negative A_V values in the latest spectral types.

Figure 16 shows the distribution of extinction of spectral-typed members earlier than M5 (solid line) and the subset of

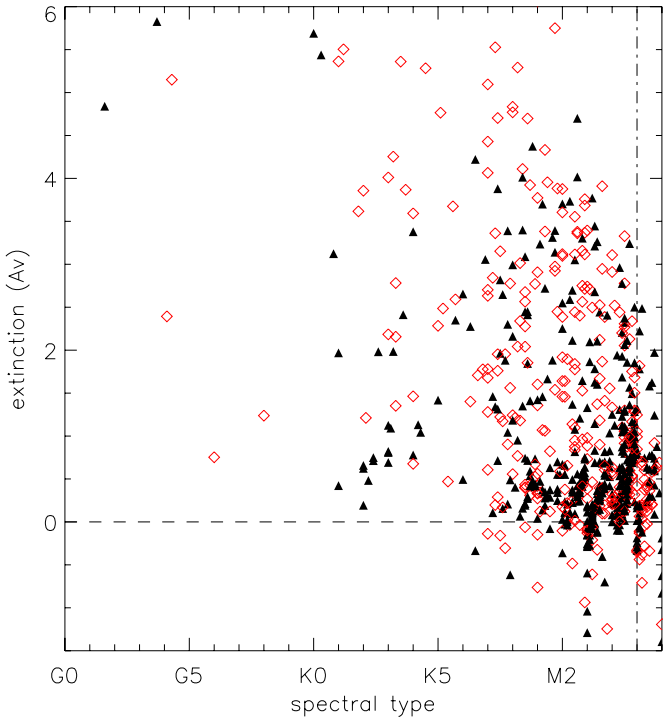

Figure 15. Extinction vs. spectral types for IR-excess objects (red open diamonds) and non-IR-excess objects (black solid triangles) estimated from $E(V-I)$, assuming the standard extinction law from Cardelli et al. (1989) for R_V of 3.1 and intrinsic colors from Kenyon & Hartmann (1995; for spectral types earlier than M4) and the young disk population in Leggett (1992; for spectral types M4 and later).

(A color version of this figure is available in the online journal.)

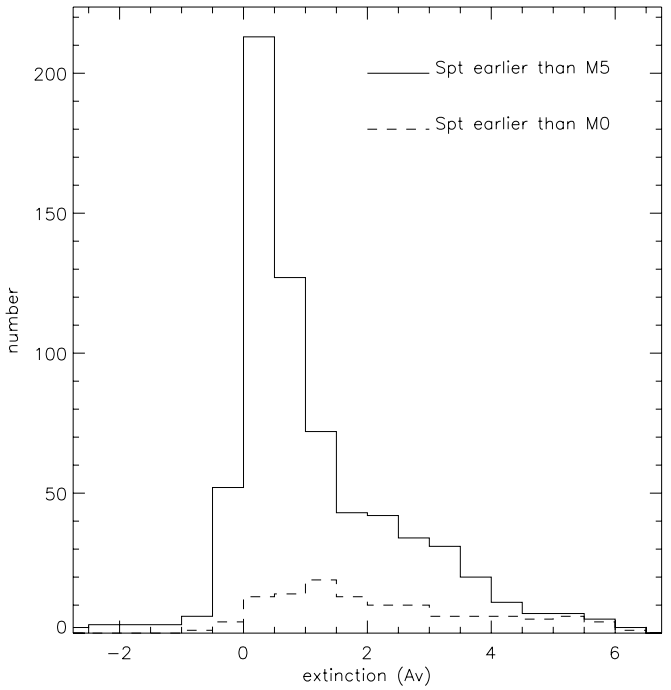

Figure 16. Distribution of extinction toward members with spectral types earlier than M5 (solid line) and members with spectral types earlier than M0 (dashed line). This illustrates that our sample does not have a uniform cutoff in extinction. The extinction is estimated from $E(V-I)$ assuming the standard extinction law from Cardelli et al. (1989) for R_V of 3.1 and intrinsic colors from Kenyon & Hartmann (1995). Stars later than M5 are not considered because of the large uncertainties in spectral typing and photometry.

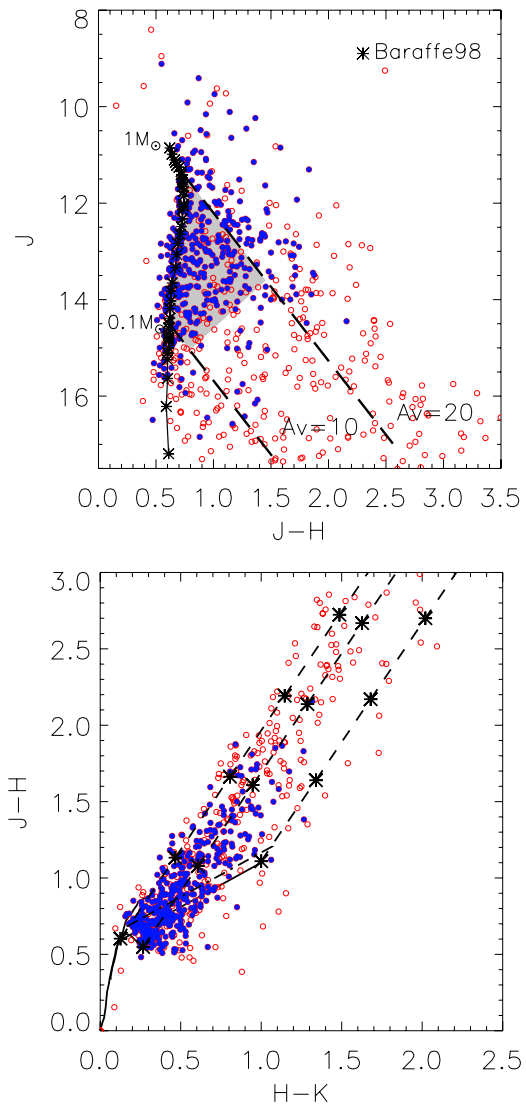

Figure 17. Top: J vs. $J - H$ color–magnitude diagram of all IR-excess objects. The objects that we spectral-typed are shown in solid circles (blue), and objects without spectral types are shown in open circles (red). Overplotted are the 3 Myr isochrone from Baraffe et al. (1998) and extinction vector from 1 $M_{\odot}$ ($A_V = 20$) and 0.1 $M_{\odot}$ ($A_V = 10$). In the shaded area, our optical spectroscopy sample is about 80% complete. Bottom: $J - H$ vs. $H - K$ color–color diagram. The two solid lines are the intrinsic colors of main sequence and giant branch (Bessell & Brett 1988). The dashed lines and the asterisks show the extinction in A_V of 5 increments. In both plots, we use the standard extinction law from Cardelli et al. (1989) for R_V of 3.1.

(A color version of this figure is available in the online journal.)

members earlier than M0 (dashed line). Stars later than M5 have large uncertainties in their spectral types and photometry and are excluded. The two distributions show that in extincted regions, our sample is biased toward more luminous objects because we did not apply an extinction cut in our sample selection.

We now turn our attention to the IR-excess population and assess what percentage of this population is highly extincted and not in our optical sample.

We use the 2MASS colors of the IR-excess disk objects to estimate the extinction and assess the completeness of our spectroscopic sample. The top panel of Figure 17 shows the J versus $J - H$ CMD of all IR-excess objects. The objects that we spectral-typed are shown in solid circles (blue), and objects without spectral types are shown in open circles (red). Overplotted are the 3 Myr isochrone from Baraffe et al. (1998) and extinction vector from 1 $M_{\odot}$ ($A_V = 20$) and 0.1 $M_{\odot}$ ($A_V = 10$). We use the isochrone from Baraffe et al. (1998) since they are appropriate for the mass range. We assume an age of 3 Myr because our optical photometry (Figure 12) shows that L1641 is approximately 3 Myr old (estimated using the Siess et al. 2000 isochrones) and the 3 Myr Baraffe et al. (1998) isochrone works the best to match up spectral type and J magnitudes. The bottom panel shows the $J - H$ versus $H - K$ color–color diagram. The two solid lines are the intrinsic colors of main sequence and giant branch (Bessell & Brett 1988). The dashed lines and the asterisks show the extinction in A_V of 5 increments. In both plots, we use the standard extinction law from Cardelli et al. (1989) for R_V of 3.1.

From the distribution of the spectral-typed objects, we found that our ability to determine spectral types is limited by both the mass (corresponding to the J magnitude) and extinction. For example, we can identify and spectral-type 1 $M_{\odot}$ stars in dense regions up to $A_V = 8$, but we can only identify and spectral-type 0.1 $M_{\odot}$ stars up to $A_V = 2$. There are 234 IR-excess sources in the shaded region of the top panel of Figure 17, and more than 80% of them (192) are spectral-typed. If we limit ourselves to objects with $A_V < 2$ for 1–0.1 $M_{\odot}$, then our spectroscopic sample is about 90% (90/110) complete. We expect similar completeness for non-excess objects. Some of the intermediate-mass and massive stars are missing as a result of the brightness limit of our spectroscopic survey, which we will address in a forthcoming paper. Of all the IR-excess objects that lie between the 0.1 $M_{\odot}$ and 1 $M_{\odot}$ line, only 60% of them have $A_V > 2$, which generally agrees with our previous finding that only half of the IR-excess stars are visible in the optical with $V < 21$.

These results show that our spectral-type distribution (Figure 10) is substantially incomplete at the latest types. This poses a problem for addressing the shape of the IMF at low masses, which we will also address in the forthcoming paper. However, from the point of view of determining whether the *high-mass* end of the IMF is deficient relative to the low-mass end, missing low-mass stars from our sample only means that our results will be underestimates of the significance of any depletion of high-mass stars.

Figure 18 shows the distribution of IR-excess objects and whether we have their spectral-type data. No spectra were obtained for objects above -6° since they are not considered part of L1641. South of -6°, we have spectral types for 50% of the disk objects. Most of the missing spectral types are due to high extinction. In particular, the aggregates of stars between $-7.^{\circ}6$ and $-6.^{\circ}8$ in declination are highly extincted (Gutermuth et al. 2011) and therefore were too faint for spectral typing.

Figure 19 shows the distribution in declination (top) and the cumulative distribution (bottom) of the optical spectroscopically confirmed members (solid lines) and the distribution of all the IR-excess disk stars (dashed lines). In low-extinction regions, we are able to classify most of the Class II and Class III stars, and the number of spectroscopic members is larger than the IR-excess sample, whereas in high-extinction regions, there are very few optical members. For example, the number of optical members is very small around decl. $= -7.^{\circ}5$ to $-6.^{\circ}8$ due to extinction.

4. DISCUSSION

4.1. Low-mass Population

In Section 3.2 we discussed our sample of optically confirmed members, including most of the moderately extincted Class II

Table 5
Sample Definition

Definition	IR Excess Disks	No IR Excess	Total Number
Spectroscopically confirmed members	406[d]	458	864
IR-excess sample from S. T. Megeath et al. (2012, in preparation)	723		723
IR-excess sample with spectral type	406[c]		406
IR-excess sample without spectral type	317		317
Class III stars with moderate extinction[a]		$\gtrsim$458	$\gtrsim$458
All known members[b]	723	458	1181
Total number of Class III stars[c]		~900	~900
Number of moderately extincted stars	406	$\gtrsim$458	~860
Total number of stars	723	~900	~1600

Notes.
[a] Estimated number from the V vs. $V-I$ CMD, minus the extrapolated foreground contamination. See Section 2.1.
[b] All known members include all spectroscopically confirmed members and the IR-excess sample without spectral type.
[c] Assuming that the Class II/Class III ratio is the same for the extincted population.
[d] This number includes eight objects that are classified as protostars, most of which are in fact flat-spectrum objects.

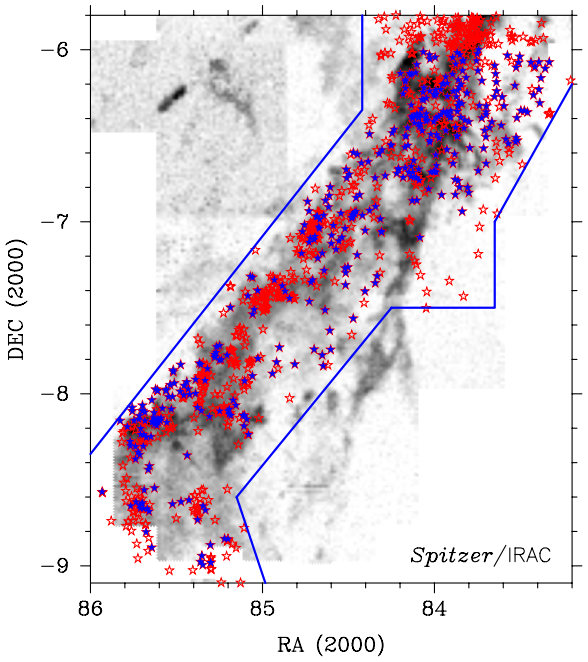

Figure 18. Same as Figure 1, but the IR-excess stars with spectral types are plotted in blue solid symbols and IR-excess stars without spectral types are plotted in red open symbols. Most of the missing spectral types are due to high extinction.

(A color version of this figure is available in the online journal.)

stars and some Class III stars that were observed serendipitously. In Section 3.4 we discussed the sample of highly extincted Class II stars that are without spectral types. In this section, we will estimate the number of Class III objects expected in L1641 from the CMD and compare this number to the number of Class III stars that we have already observed. Table 5 gives the definitions of the various populations and their numbers. (Note that numbers with ~ signs are estimates).

We noted that most of the IR-excess stars fall in a small region on the optical CMD (Figure 4) between the top two parallel lines (described in Section 2.1). We expect that the Class III objects have similar ages and distances and therefore fall in the same region of the CMD. However, not all the non-IR-excess objects in this region are members. To estimate the fraction of the non-members in the non-IR-excess sample, we use the strip 1 mag below the YSO region as a reference to estimate the number of foreground contaminants in the YSO region. Assuming no foreground extinction and uniform stellar density of foreground stars, the distribution of foreground stars in a given magnitude band is proportional to $10^{0.6m}$ (see Section 3.6 in Binney et al. 2000). Therefore, the number of foreground stars in the YSO region is predicted to be $10^{-0.6} + 10^{-1.2}$ times the number of foreground stars in the reference strip.

We restrict our extrapolation to a $V-I$ range of 2–3.5 as this is the only portion where we have data for both the reference and the YSO region. We identified 514 stars in the reference strip between $V-I$ of 2 and 3.5 (only a very small fraction of which are members). The estimated contamination in the YSO region is therefore $514 \times (10^{-0.6} + 10^{-1.2}) \approx 162$ stars. There are 496 non-IR-excess objects in the YSO region between $V-I$ of 2 and 3.5. We therefore estimate that about 33% of the non-excess stars in the YSO strip are non-members.

The entire YSO strip from $V-I$ of 0.5 to 4 has 772 non-excess stars. If we take the same contamination rate of 33%, we estimate that $772 \times (1\%–33\%) \sim 520$ of these non-excess stars are members. This agrees roughly with the number of Class III objects (458) that we confirmed spectroscopically and shows that we have identified the vast majority of the Class III objects subject to our extinction limits.

Approximately half (347 out of 723) of the IR-excess objects are identified in the optical photometry. If we further assume that the ratio of Class II to Class III stars is constant even for the more extincted population, then we can estimate that there are $458 \times 2 \sim 900$ Class III objects. The total population of Class II + Class III stars in L1641 would then be ~1600.

The above calculation, of course, is a very rough estimate and depends on our assumptions. First, we assumed that the foreground stars are all main-sequence stars and are uniformly distributed. We have also implicitly assumed that the Class II to Class III ratio is constant for all spectral types, while the observed disk frequency is a function of spectral type (see, e.g., Lada et al. 2006); however, this is probably a reasonable assumption for the majority of our members, as the disk frequency seems to decrease most strongly for stars earlier than M. The assumption that the disk frequency is the same for the extincted population can also be problematic. The *Spitzer*/IRAC survey has found that Class II objects in L1641 are more distributed spatially compared to the Class I stars (Allen et al. 2007); similarly, it may be that the Class III objects are more

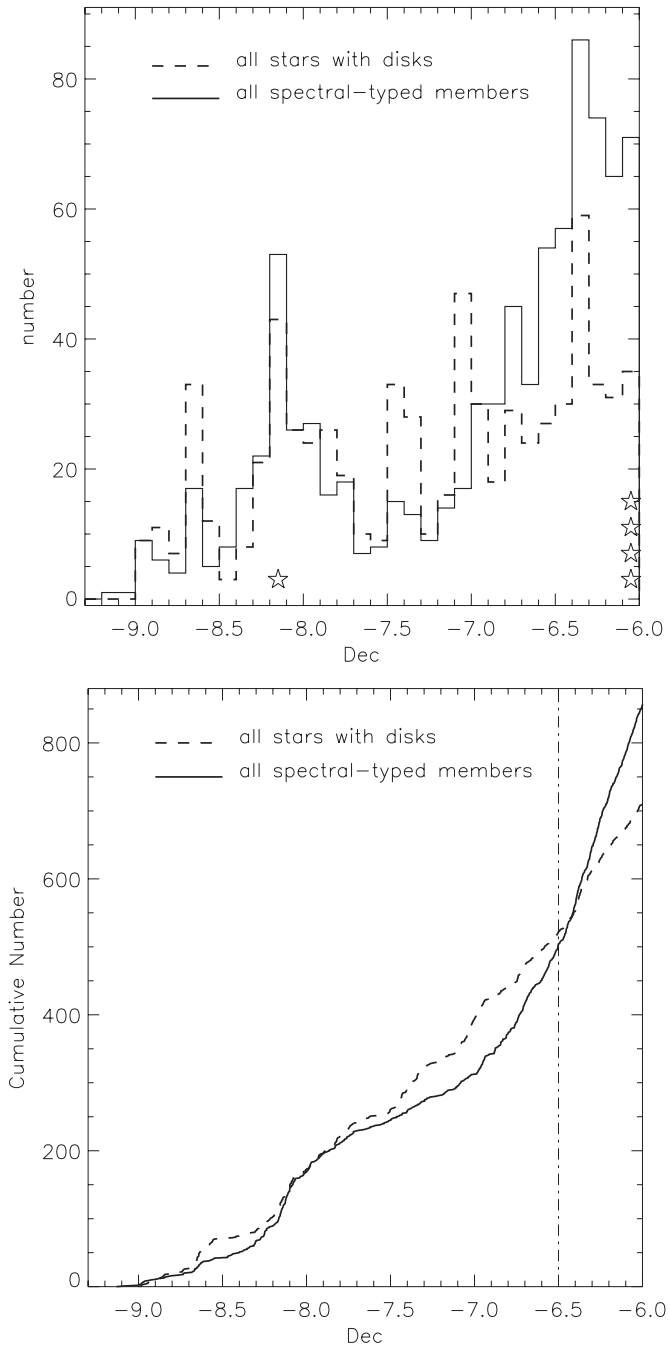

Figure 19. Top: distribution of spectroscopically confirmed, spectral-typed YSOs (solid line) and all stars with disks (dashed line). The star symbols show the number of B0–B4 stars in each bin. The low number of spectral-typed stars around decl. = −7.°5 to − 6.°8 is a result of high extinction in this declination range. Bottom: cumulative distribution of stars along increasing declination. The horizontal dash-dotted line represents a more strict cutoff of L1641 at decl. = −6.°5 (see Section 4.3).

distributed and have lower extinction systematically than the Class II stars. S. T. Megeath et al. (2012, in preparation) estimated a disk fraction of 70%–80% in denser regions of L1641 by using off fields to subtract out the number of contaminating stars, higher than the disk fraction we found for moderately extincted stars. Therefore, assuming the same disk fraction could lead to an overestimate of the number of Class III stars.

We can compare the number of low-mass stars in L1641 to the results from surveys of the ONC. The ONC region has been

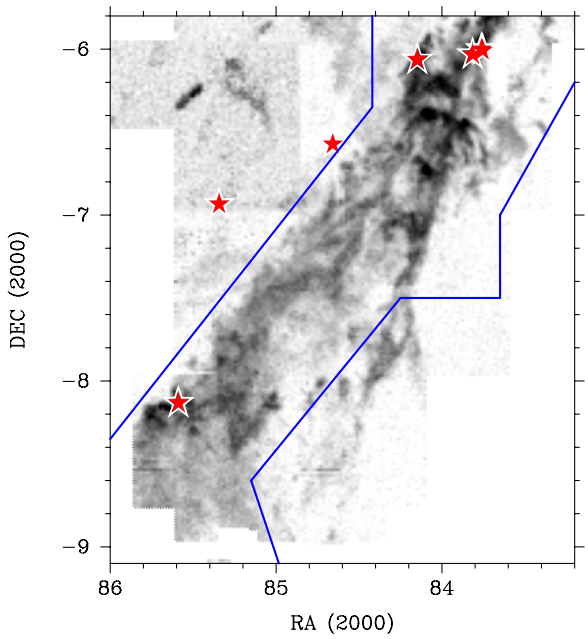

Figure 20. Positions of known B0–B4 stars near L1641 overlaid on the ^{13}CO map (Bally et al. 1987). The blue solid line outlines the *Spitzer*/IRAC fields. The spectral-type information is taken from the spectral-type compilation by Skiff (2010). There are no O stars in this region.

(A color version of this figure is available in the online journal.)

surveyed multiple times both in the IR and in the optical. The number of sources found highly depends on the area and depth of the specific surveys. Most of the IR surveys go much deeper than 2MASS, which makes comparing the number of sources more difficult. The optical survey of Da Rio et al. (2010) is probably the most comparable to ours since they have a 50% *V*-band completeness limit of 20.8. In an area of 34′ × 34′ they identified ∼1500 stars that are present in both the *V* and *I* bands. Hillenbrand (1997) also has a similar survey area and found a similar number of objects. Therefore, we conclude that L1641 contains a comparable number of stars as the half-degree field centered on the ONC to within a factor of two. This suggests that a direct comparison of the stellar IMFs in the two regions can be statistically meaningful.

4.2. High-mass Population

With an idea of the number and spatial distribution of low-mass stars in L1641, we can now look into the high-mass end of the IMF. We search for known early-type stars in L1641 in the catalog of spectral types compiled by Skiff (2010). There are no O stars in the area shown, and the known early B-type (B0–B4) stars are shown in Figure 20, overlaid on the ^{13}CO map (Bally et al. 1987). Table 6 lists the positions, spectral types, and photometry of these stars. In the case of spectral classifications from multiple sources, the most recent classification is used. There are a total of seven early B stars in this region. Four of the early B stars (1–4 in Table 6) are on the northern tip of the cloud and potentially denote the outer regions of the ONC; two other stars (5 and 6) are not associated with the cloud if seen in ^{13}CO emission but could be associated with the lower-density gas probed by the near-IR (2MASS) extinction map. Since we do not have information on the low-mass population in their surroundings and they are not clearly associated with L1641, we will not consider these two stars in the IMF analysis. The other early B star (7) is the B4 star near (R.A., decl.) = (5:42:21.3,

Table 6
List of Early B-type Stars in L1641

No.	R.A. (J2000)	Decl. (J2000)	Name	Spectral Type[a]	V[b] (mag)	$B-V$[b] (mag)	In *Spitzer* Field?[c] Y or N
1	83.7542	−6.00928	HD 36959	B1.5V[d]	5.68	−0.21	Y
2	83.7612	−6.00203	HD 36960	B0.5V[e]	4.79	−0.25	Y
3	83.8156	−6.03275	HD 37025	B2/3V[f]			Y
4	84.1487	−6.06475	HD 37209	B3IV[g]	5.72	−0.22	Y
5	84.6582	−6.57397	HD 37481	B2V[h]	5.96	−0.22	N
6	85.3434	−6.93519	HD 37889	B2.5Vsn[e]	7.65	−0.1	N
7	85.5888	−8.13339	HD 38023	B4V[i]	8.88	0.33	Y

Notes.
[a] Most recent spectral type from Skiff (2010).
[b] Optical photometry from Warren & Hesser (1977).
[c] The position on the sky is within the *Spitzer* field. We use the *Spitzer* field as a proxy of the main body of the cloud.
[d] The spectral-type information comes from Walborn & Fitzpatrick (1990).
[e] The spectral-type information comes from Abt & Levato (1977).
[f] The spectral-type information comes from Derviz (1983).
[g] The spectral-type information comes from Abt (2008).
[h] The spectral-type information comes from Zorec et al. (2009).
[i] The spectral-type information comes from Racine (1968).

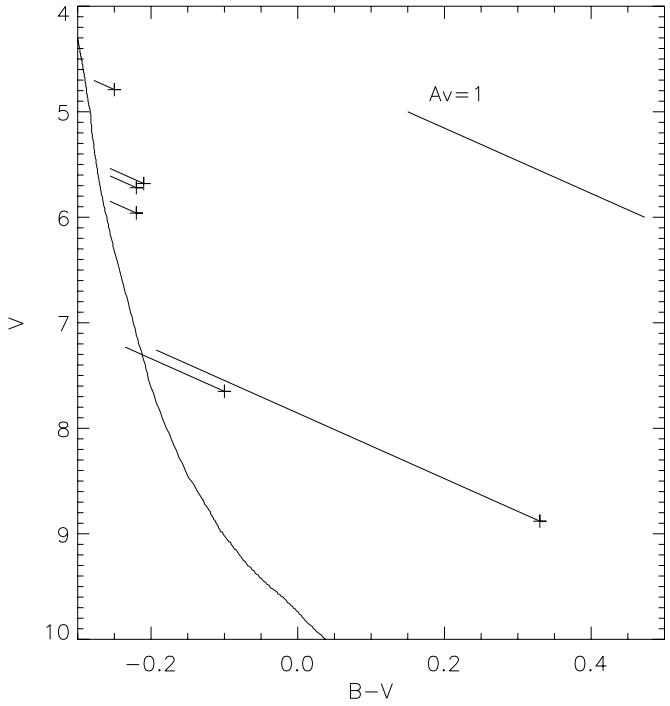

Figure 21. V vs. $B-V$ CMD of B-type stars near L1641 (shown in Figure 20). The photometry is taken from Warren & Hesser (1977). The curved solid line is the ZAMS from Schaller et al. (1992; Geneva tracks). Note that B and V photometry is not available for all B-type stars. The solid line extending from each star shows its dereddened position on the CMD, where the extinction is calculated from the $E(B-V)$ color excess.

−08:08:00) (Racine 1968). Figure 21 shows the V versus $B-V$ CMD of these early B stars with photometry from Warren & Hesser (1977) with the ZAMS from Schaller et al. (1992) (Geneva tracks) overplotted. The dereddened position of each star is also shown, where the extinction is calculated from the $E(B-V)$ color excess. All the known early B stars are consistent with the ZAMS at the distance of 420 pc, which means they are likely associated with Orion A.

From Figure 21, we found that all of the known early B stars have small extinctions of $A_V < 2$, which is a result of the depth of the Warren & Hesser (1977) photometry. It is therefore possible that there are embedded O or early B stars that have not been found. However, based on the existing *Spitzer* survey (S. T. Megeath et al. 2012, in preparation), it is unlikely that we miss an early B star. Evolved O or early B stars would have blown away materials nearby in a manner similar to the B4 star near (R.A., decl.) = (5:42:21.3, −08:08:00) and therefore will not have high extinction. The reflection nebula near the B4 star is the only one seen in our field, which supports that there are no evolved early B stars. (Note that there is another reflection nebula, powered by a potentially massive star farther south, outside of the fields of our optical studies.) On the other hand, if there were unevolved, highly extincted early B stars, they would probably heat up the dust nearby and be identified as bright IR-excess sources by the *Spitzer* survey. We first examine possible high-mass disk objects in the J versus $J-H$ CMD (top panel of Figure 17). The brightest star in the J band is on the upper left corner and has a spectral type of A1. A few other stars appear to have similar mass and are more extincted, but they all have similar masses according to the diagram. The only exception is the FU Ori star V883 Ori (with $J = 9.25$ and $J-H = 2.49$), which is dominated by accretion luminosity. We then examine the protostars that have large bolometric luminosities. The most luminous protostar in L1641 is located at (R.A., decl.) = (5:40:27.4,−7:27:30) in one of the high-extinction clumps. It has $L \sim 490\ L_\odot$ (Kryukova et al. 2012) and, according to the Siess et al. (2000) isochrones, has a mass less than 7 $M_\odot$.

4.3. Comparing the High-mass IMF of L1641 to Analytical IMFs

In Section 4.2, we discussed the high-mass population in L1641 from a literature search. In our following analysis, we assume that there are no other early B stars in the region. All but one of the early B stars are in the northern region contiguous with the ONC region. This raises the question of how we should define the region in which we construct the IMF. We need to adopt a more conservative definition and limit our sample to stars from a lower declination. This also means we have to compromise for a smaller sample size. Figure 19 shows that

Table 7
Samples by Region and IMF Probabilities

Region	n (Sample Size)	$M_{\max}$[a]	$p = 1 - \Sigma(M_{\max})$[b]	$E(> M_{\max})$[c]	P (No Stars Greater than $M_{\max}$)[d]
L1641	Spectral-typed members 864	B0.5V	Chabrier05 3.74×10^{-3}	3.2	0.039
Decl. $< -6°$		(16 $M_\odot$)	Kroupa01 2.77×10^{-3}	2.4	0.091
	Total known members[e] 1181	B0.5V	Chabrier05 3.74×10^{-3}	4.4	0.012
		(16 $M_\odot$)	Kroupa01 2.77×10^{-3}	3.3	0.038
Decl. $= -6°$ to $-6.^\circ5$	Spectral-typed members 364	B0.5V	Chabrier05 3.74×10^{-3}	1.4	0.26
		(16 $M_\odot$)	Kroupa01 2.77×10^{-3}	1.0	0.36
	Total known members[e] 419	B0.5V	Chabrier05 3.74×10^{-3}	1.6	0.20
		(16 $M_\odot$)	Kroupa01 2.77×10^{-3}	1.2	0.31
Decl. $< -6.^\circ5$	Spectral-typed members 500	B4V	Chabrier05 1.26×10^{-2}	6.3	1.8×10^{-3}
		(7 $M_\odot$)	Kroupa01 8.55×10^{-3}	4.3	1.4×10^{-2}
	Total known members[e] 762	B4V	Chabrier05 1.26×10^{-2}	9.6	6.4×10^{-5}
		(7 $M_\odot$)	Kroupa01 8.55×10^{-3}	6.5	1.4×10^{-3}

Notes.
[a] Most massive star observed in this region.
[b] The probability that a random star drawn from the IMF is more massive than $M_{\max}$.
[c] Expected number of stars more massive than $M_{\max}$. $E(> M_{\max}) = np$.
[d] Drawing n stars from the given IMF, the probability of getting no stars more massive than $M_{\max}$. $P = (1 - p)^n$.
[e] Total known members include spectral-typed members and IR-excess members without spectral type.

a large number of the confirmed members lie in the northern end of the cloud and that our sample size will be considerably smaller if we consider only the members farther south. We need to carefully choose a cutoff for our L1641 sample.

Here we discuss whether this lack of high-mass stars is statistically significant with the following two approaches: (1) considering the entire L1641 region south of $-6°$ and (2) considering only the stars south of $-6.^\circ5$. For comparison, we also consider the region between $-6°$ and $-6.^\circ5$, which is a relatively higher density region in L1641 and contains four early B stars. Given the sample size n and the mass of the most massive star in the region $M_{\max}$, we can then calculate how unlikely it is that this sample is drawn from analytic IMF models. Here, we only consider the Chabrier (2005) and Kroupa (2001) IMFs. The Chabrier (2003) IMF gives results that are in between the two IMFs discussed here.

First, we normalize the IMFs between 0.1 and 120 $M_\odot$. The Chabrier (2005) IMF can be written as

$$\xi(\log m) = \begin{cases} = A \exp\left\{-\frac{(\log m - \log 0.25)^2}{2\times(0.55)^2}\right\}, & 0.1\,M_\odot < m < 1\,M_\odot, \\ = 0.549A\, m^{-1.35}, & m \geqslant 1\,M_\odot, \end{cases} \quad (1)$$

where $A \sim 0.959$ normalizes the total number to unity.

The Kroupa (2001) IMF can be written as

$$\xi(m) \begin{cases} = 2A\, m^{-1.3}, & 0.1\,M_\odot < m < 0.5\,M_\odot, \\ = A\, m^{-2.3}, & m \geqslant 0.5\,M_\odot, \end{cases} \quad (2)$$

where the normalization constant $A \sim 0.1431$.

The cumulative distribution function is

$$\Sigma(M) = \int_{\log(m=0.1\,M_\odot)}^{\log M} \xi(\log m) d\log m = \int_{m=0.1\,M_\odot}^{M} \xi(m) dm. \quad (3)$$

The probability that a randomly sampled star from this IMF is more massive than $M_{\max}$ is $p = 1 - \Sigma(M_{\max})$. In a population of n stars, the expected number of stars more massive than $M_{\max}$ is $E(> M_{\max}) = np$. The probability that the most massive star is below $M_{\max}$ is $P = (1 - p)^n$.

Table 7 lists the sample size n, the most massive star in the region $M_{\max}$, and $p = 1 - \Sigma(M_{\max})$, $E(> M_{\max}) = np$ for both Chabrier (2005) and Kroupa (2001) IMFs. Note that here we consider two sample sizes: spectral-typed members and total known members, which is the sum of spectral-typed members and the IR-excess members that are too extincted for optical spectroscopy. Generally, the Chabrier (2005) IMF gives a higher number of high-mass stars and therefore is less likely to find no high-mass stars.

If we consider the entire L1641 region south of $-6°$, the most massive star is a B0.5V star (corresponding to $M_{\max} \sim 16\,M_\odot$). We expect to see 2.4–4.4 stars more massive than the B0.5V star in such a population. If the populations are randomly drawn, the probability of not finding any star more massive than 16 $M_\odot$ is quite low (0.012–0.091). Therefore, this population has fewer high-mass stars compared to the analytic IMF models, but the result is not very statistically significant.

If we consider only the region between $-6°$ and $-6.^\circ5$, the most massive star in this region (B0.5V) is compatible with random sampling of both the analytical IMFs.

By limiting our sample to stars south of $-6.^\circ5$ and on the cloud (i.e., within the *Spitzer* survey area), we can ensure that our sample is not confused with stars from the ONC. There are no stars earlier than B4 (corresponding to $M_{\max} \sim 7\,M_\odot$) in this sample. We expect to see 4.3–9.6 stars more massive than the B4V star in such a population. If the populations are randomly drawn, the probability of not finding any star more massive than 7 $M_\odot$ is very low (1.4×10^{-2}–6.4×10^{-5}). If we consider only the 500 members with optical spectral types, the population is incompatible with the analytic IMFs to a 2σ–3σ level; if we further include the 262 IR-excess members without optical spectral type, the population is incompatible with the analytic IMF to a 3σ–4σ level.

Even though we currently cannot constrain the total number of highly extincted stars, the total population will only be larger if we consider highly extincted Class III stars. Assuming a

complete sample of early B stars and the lower limit of low-mass stars, the probabilities we calculated above are upper limits. Therefore, the existence of highly extincted low-mass stars will only strengthen and not weaken our conclusions. On the other hand, our conclusion relies very strongly on the assumption that there are no highly extincted high-mass members, especially stars earlier than B4 in the region south of decl. $= -6.^{\circ}5$. We also want to point out that the expected number of high-mass stars varies greatly for different IMF models due to their discrepancies in the low-mass end. The low-mass IMF is less well studied, and the discrepancies in the models can be viewed as an indication of the uncertainties.

Since we do not yet have a complete analysis of the high-mass and intermediate-mass stars in L1641, we choose not to present an H-R diagram of the low-mass sample alone. We will present the high- to intermediate-mass sample in a forthcoming paper, in which we will be able to construct a full IMF (down to M3) of L1641 and compare it to that of the ONC.

5. CONCLUSIONS

We conducted an optical photometric and spectroscopic survey of L1641 to test whether IMF varies with the environmental densities. Our spectroscopic sample consists of IR-excess objects selected from the *Spitzer*/IRAC survey and optical photometry and non-excess objects selected from optical photometry. We have spectral-typed 406 IR-excess members. We have also identified and spectral-typed 458 non-excess YSOs and 98 probable members through Li absorption and Hα emission. Our sample is limited by extinction and stellar mass in a complicated way, but overall we are able to spectral type about 90% of Class II and Class III YSOs between 0.1 and 1 $M_{\odot}$ with $A_V \lesssim 2$. The number of spectroscopically confirmed Class III objects is also consistent with the number of Class III objects estimated from extrapolation of the V versus $V - I$ CMD.

Assuming that the Class III/Class II ratio is the same for the more extincted population, we estimate the total number of Class II and Class III stars in L1641 to be around 1600, including 723 Class II objects from the *Spitzer* survey and ~900 Class III stars.

The total number of stars in L1641 is comparable within a factor of two to the number of stars used to construct the IMF in the ONC, even though the number depends on how our L1641 sample is defined. The optical photometry shows that the ONC and L1641 are of similar age, with L1641 being slightly older by ~1 Myr, indicating that any late O to early B star should still be on the main sequence. Assuming that we know all the early B stars in L1641, we compare the high-mass IMF to the standard analytical models. Compared to the standard models of the IMF, L1641 is deficient in O and early B stars to a 3σ–4σ significance level. We will make further improvements to our sample to better constrain the extincted population and compile a complete sample of B stars in a forthcoming paper, and then we will be able to make a direct comparison with the ONC.

We thank the referee for helpful suggestions to improve the manuscript. W.H. and L.H. acknowledge the support of NSF Grant AST-0807305 and the Origins Grant NNX08AI39G. This paper uses data obtained at the MMT Observatory, a joint facility of the Smithsonian Institution and the University of Arizona, and the 6.5 m Magellan Telescopes located at Las Campanas Observatory, Chile. This paper uses data products produced by the OIR Telescope Data Center, supported by the Smithsonian Astrophysical Observatory.

Facilities: MMT (Hectospec), Magellan:Baade (IMACS), Hiltner (OSMOS), Spitzer (IRAC), FLWO:2MASS.

REFERENCES

Abt, H. A. 2008, ApJS, 176, 216
Abt, H. A., & Levato, H. 1977, PASP, 89, 797
Allen, L., Megeath, S. T., Gutermuth, R., et al. 2007, in Protostars and Planets V, ed. B. Reipurth, D. Jewitt, & K. Keil (Tucson, AZ: Univ. Arizona Press), 361
Allen, L. E. 1995, PhD thesis, Univ. Massachusetts, Amherst
Allen, L. E., & Davis, C. J. 2008, in Low Mass Star Formation in the Lynds 1641 Molecular Cloud, ed. B. Reipurth (San Francisco, CA: ASP), 621
Bally, J., Lanber, W. D., Stark, A. A., & Wilson, R. W. 1987, ApJ, 312, L45
Baraffe, I., Chabrier, G., Allard, F., & Hauschildt, P. H. 1998, A&A, 337, 403
Bastian, N., Covey, K. R., & Meyer, M. R. 2010, ARA&A, 48, 339
Bessell, M. S., & Brett, J. M. 1988, PASP, 100, 1134
Bigelow, B. C., & Dressler, A. M. 2003, Proc. SPIE, 4841, 1727
Binney, J., Merrifield, M., & Wegner, G. A. 2000, Am. J. Phys., 68, 95
Briceno, C., Hartmann, L. W., Stauffer, J. R., et al. 1997, AJ, 113, 740
Cardelli, J. A., Clayton, G. C., & Mathis, J. S. 1989, ApJ, 345, 245
Chabrier, G. 2003, PASP, 115, 763
Chabrier, G. 2005, in The Initial Mass Function 50 Years Later, ed. E. Corbelli, F. Palla, & H. Zinnecker (Astrophysics and Space Science Library, Vol. 327; Dordrecht: Springer), 41
Da Rio, N., Robberto, M., Soderblom, D. R., et al. 2009, ApJS, 183, 261
Da Rio, N., Robberto, M., Soderblom, D. R., et al. 2010, ApJ, 722, 1092
Derviz, T. E. 1983, Trudy Astronomicheskoj Observatorii Leningrad, 38, 62
Fabricant, D., Fata, R., Roll, J., et al. 2005, PASP, 117, 1411
Fang, M., van Boekel, R., Wang, W., et al. 2009, A&A, 504, 461
Gâlfalk, M., & Olofsson, G. 2008, A&A, 489, 1409
Gutermuth, R. A., Megeath, S. T., Myers, P. C., et al. 2009, ApJS, 184, 18
Gutermuth, R. A., Pipher, J. L., Megeath, S. T., et al. 2011, ApJ, 739, 84
Hernández, J., Calvet, N., Briceño, C., Hartmann, L., & Berlind, P. 2004, AJ, 127, 1682
Hillenbrand, L. A. 1997, AJ, 113, 1733
Hillenbrand, L. A., & Hartmann, L. W. 1998, ApJ, 492, 540
Kenyon, S. J., & Hartmann, L. 1995, ApJS, 101, 117
Kim, M. K., Hirota, T., Honma, M., et al. 2008, PASJ, 60, 991
Koenigl, A. 1991, ApJ, 370, L39
Kroupa, P. 2001, MNRAS, 322, 231
Kryukova, E., Megeath, S. T., Gutermuth, R. A., et al. 2012, arXiv:1204.1535
Lada, C. J., Muench, A. A., Luhman, K. L., et al. 2006, AJ, 131, 1574
Leggett, S. K. 1992, ApJS, 82, 351
Luhman, K. L., Mamajek, E. E., Allen, P. R., & Cruz, K. L. 2009, ApJ, 703, 399
Martini, P., Stoll, R., Derwent, M. A., et al. 2011, PASP, 123, 187
Menten, K. M., Reid, M. J., Forbrich, J., & Brunthaler, A. 2007, A&A, 474, 515
Mink, D. J., Wyatt, W. F., Caldwell, N., et al. 2007, in ASP Conf. Ser. 376, Astronomical Data Analysis Software and Systems XVI, ed. R. A. Shaw, F. Hill, & D. J. Bell (San Francisco, CA: ASP), 249
Muench, A. A., Lada, E. A., Lada, C. J., & Alves, J. 2002, ApJ, 573, 366
Racine, R. 1968, AJ, 73, 233
Rebull, L. M., Koenig, X. P., Padgett, D. L., et al. 2011, ApJS, 196, 4
Robberto, M., Soderblom, D. R., Scandariato, G., et al. 2010, AJ, 139, 950
Schaller, G., Schaerer, D., Meynet, G., & Maeder, A. 1992, A&AS, 96, 269
Siess, L., Dufour, E., & Forestini, M. 2000, A&A, 358, 593
Skiff, B. A. 2010, VizieR Online Data Catalog, 1, 2023
Stauffer, J. R., Hartmann, L. W., Prosser, C. F., et al. 1997, ApJ, 479, 776
Stoll, R., Martini, P., Derwent, M. A., et al. 2010, Proc. SPIE, 7735, 77354L
Walborn, N. R., & Fitzpatrick, E. L. 1990, PASP, 102, 379
Warren, W. H., Jr., & Hesser, J. E. 1977, ApJS, 34, 115
Weidner, C., Kroupa, P., & Bonnell, I. A. D. 2010, MNRAS, 401, 275
White, R. J., & Basri, G. 2003, ApJ, 582, 1109
Zorec, J., Cidale, L., Arias, M. L., et al. 2009, A&A, 501, 297